

PREPARED FOR SUBMISSION TO JHEP

Collider Constraints and Prospects of a Scalar Singlet Extension to Higgs Portal Dark Matter

Grace Dupuis

*Department of Physics, McGill University,
Rue University, Montréal, Québec, Canada*

E-mail: dupuisg@physics.mcgill.ca

ABSTRACT: This work considers an extension of the Standard Model (SM) Higgs sector by a real, scalar singlet field, including applicability to a dark matter (DM) model with the addition of a Yukawa coupling to a fermionic dark matter candidate. The collider signatures and constraints on the mixed two-Higgs scenario are determined, including limits from Higgs production signals and exclusion searches, as well as constraints arising from the Higgs total and invisible widths. As there is overwhelming Higgs data which is consistent with a SM scenario, the case in which an additional scalar has evaded detection is further explored in the context of Higgs precision measurement. The discovery reach and prospective signatures of the model at a proposed linear collider are investigated, with particular focus on the Higgs triple coupling, and di-Higgs production processes.

Contents

1	Introduction	1
2	Model	3
3	New Decay Channels	5
3.1	Partial Widths	5
3.2	Scalar Couplings	6
3.3	Three-Body Decays	6
4	LHC Limits	10
4.1	Higgs Signal Strength and Exclusion Searches	10
4.2	Invisible Signals	12
4.3	Total Higgs Width	12
5	ILC Prospects	14
5.1	Di-Higgs Processes	17
6	Direct Detection	22
7	Conclusion	23
A	Di-Higgs Production Diagrams	24

1 Introduction

The discovery of the Higgs boson at the Large Hadron Collider (LHC) is one of the most significant scientific achievements of late. By finally providing long-awaited evidence of the previously undiscovered scalar sector of the Standard Model (SM), this groundbreaking result has sparked much excitement. Not only does this discovery verify the well-established fundamental theory of particle physics, it also presents new possibilities to probe physics beyond the Standard Model. Although this result is a major achievement in the field of particle physics, the Higgs sector still remains largely unexplored. Specifically, it has yet to be determined whether the discovered scalar is indeed the Higgs boson of the Standard Model, or a piece of some extended theory. Such a question lies under the realm of Higgs precision measurements. Future experiments, reaching higher energies and employing advancing techniques will shed light on precision aspects such as the Higgs CP nature, its self-couplings and couplings to electroweak vector bosons, and possible deviations from the Standard Model that may indicate a larger Higgs sector.

As successful as the Standard Model has proven to be, there are still missing pieces, one of which is the failure to account for the identity of dark matter (DM) as a particle species. Extensions of the SM scalar sector lend themselves to models of DM, through potential DM candidates and/or new mediators bridging the dark and visible sectors. The study presented here considers one of the simplest such extensions — the addition of a scalar singlet field, which couples to a fermionic DM candidate. The scalar singlet extension is attractive in its simplicity, hence, similar models have been studied extensively in the literature. The implications on the Higgs sector of a pure scalar singlet extension have been investigated [1–5], as well as the viability of such a model in a dark matter context [6–9], with subtle distinctions. There is a wide range of models which contain a new scalar singlet, including similar studies of the implications of an additional Higgs-like scalar, with varying instances of the scalar potential and Higgs-scalar interaction terms [10, 11].

Often such models, which are typically referred to as Higgs portal, couple the SM field directly to a DM candidate [12, 13]. Studies of scalar singlet extensions also exist which take the additional scalar as the DM candidate, as it is protected under a Z_2 symmetry [14–17]. The new scalar here acquires a vacuum expectation value (vev) and mixes with the SM Higgs field, giving two scalar mediators that act as the portal to the dark fermion. The case of a dark fermion with its SM interactions mediated by a new scalar or pseudoscalar has also been considered, but in the context of a bottom-up, effective field theory (EFT) approach, without considering the mixing of the scalar and SM Higgs [18], or embedded in a more complex model with additional extensions [19].

In the following study, a scalar singlet extension is investigated, with applicability to a model of dark matter. Focus is placed on the collider implications of the mixing in the Higgs sector, particularly the prospective influence of the additional scalar in Higgs precision measurements at the proposed International Linear Collider (ILC). The applicability of the model in a dark matter context is addressed in associated invisible signatures, and compatibility with direct detection (DD) limits. As current LHC data is consistent with a SM Higgs, it is vital to further consider the scenario in the context of future experiments, in the case where an additional Higgs-like scalar has evaded detection. Under this assumption, the discovery potential at a proposed linear collider is explored. A lepton collider is advantageous in possessing greater sensitivity to Higgs precision measurements, to which the LHC may not be sensitive. It is discussed how a precision environment may probe the scalar parameters of the model, and what distinguishing features may be observable. In particular, the study focuses on the Higgs self-coupling through double Higgs production processes.

This work is structured as follows. The model and its parametrization are presented in section 2. As the implications of new decay modes are examined, expressions for the new decay widths are given in section 3. The LHC constraints are presented in section 4, including both a review of Higgs exclusion searches and measured signals, as well as specific invisible searches. The topic of discovery reach and projected limits at a future linear collider is explored in section 5. The compatibility with direct detection data is addressed in section 6. A concluding discussion is then given on the viability and prospects of the model.

2 Model

The scalar sector of the SM is supplemented with an additional real scalar field, which is a singlet under the SM gauge group and couples to a fermionic dark matter candidate via a Yukawa term. The additional scalar acquires a vev in the same way as the familiar SM Higgs field, thereby inducing mixing between the new scalar and the Higgs. The model is parametrized as follows.

The scalar potential is modified, according to

$$V(\Phi_1, \phi_2) = \lambda_1(\Phi_1^\dagger \Phi_1 - v_1^2/2)^2 + \frac{\lambda_2}{4}(\phi_2^2 - v_2^2)^2 + \frac{\lambda_{12}}{2}(\Phi_1^\dagger \Phi_1 - v_1^2/2)(\phi_2^2 - v_2^2), \quad (2.1)$$

where Φ_1 is the SM Higgs doublet and v_1 is equivalent to the SM Higgs vev, specifically $v_1 = 246$ GeV; ϕ_2 is the additional field. As the new field is a singlet under the SM gauge, the familiar symmetry breaking mechanism, with respect to the electroweak sector, is unchanged. Hence, the SM Higgs vev and other electroweak parameters are the same as in the SM case.

A Yukawa interaction is introduced, coupling a dark, vector-like fermion to the scalar singlet field, as described by the following interaction Lagrangian:

$$\mathcal{L}_{\text{dark}} \supset -\frac{1}{2}\phi_2 (g_L \bar{\psi}_L \psi_L^c + g_R \bar{\psi}_R \psi_R^c) + \text{h.c.} \quad (2.2)$$

There is a discrete symmetry in this case by which the fields transform as

$$\begin{aligned} \psi_L &\rightarrow i\psi_L \\ \psi_R &\rightarrow -i\psi_R \\ \phi_2 &\rightarrow -\phi_2. \end{aligned}$$

This symmetry forbids both a bare Dirac mass term, as well as any terms of odd order in ϕ_2 in the scalar potential. Eq. 2.1 represents the most general scalar potential consistent with the symmetry.

Both scalar fields are allowed to acquire vevs,

$$\Phi_1 \rightarrow \frac{1}{\sqrt{2}} \begin{pmatrix} 0 \\ v_1 + h_1(x) \end{pmatrix}, \quad \phi_2 \rightarrow v_2 + h_2(x). \quad (2.3)$$

Beginning with the scalar sector, after diagonalizing the mass terms, one finds the following mass eigenvalues:

$$m_{H,S}^2 = (\lambda_1 v_1^2 + \lambda_2 v_2^2) \pm \sqrt{(\lambda_1 v_1^2 - \lambda_2 v_2^2)^2 + (\lambda_{12} v_1 v_2)^2}, \quad (2.4a)$$

or

$$m_S^2 = m_H^2 \pm \delta m^2; \quad \delta m^2 = 2\sqrt{(\lambda_1 v_1^2 - \lambda_2 v_2^2)^2 + (\lambda_{12} v_1 v_2)^2}. \quad (2.4b)$$

with mass eigenstates given by

$$\begin{pmatrix} H \\ S \end{pmatrix} = \begin{pmatrix} c_{\theta_h} & -s_{\theta_h} \\ s_{\theta_h} & c_{\theta_h} \end{pmatrix} \begin{pmatrix} h_1 \\ h_2 \end{pmatrix}. \quad (2.5)$$

Here c_{θ_h} and s_{θ_h} denote $\cos \theta_h$ and $\sin \theta_h$ respectively. The mixing angle is given by the following expression:

$$\tan 2\theta_h = \frac{-\lambda_{12}v_1v_2}{\lambda_1v_1^2 - \lambda_2v_2^2} \quad (2.6)$$

with $\theta_h \in [-\pi/2, \pi/2]$. H is taken to be the recently discovered Higgs boson, with mass fixed at $m_H = 125.09$ GeV [20], and the mass of the additional scalar is allowed to be either lighter or heavier than H .

The scalar sector is described by three additional parameters — the vev of the singlet field, the mass of the new scalar, and the scalar-Higgs mixing angle, $\{v_2, m_S, \theta_h\}$. In terms of these parameters, the potential coefficients are

$$\lambda_1 = \frac{1}{2v_1^2} (c_{\theta_h}^2 m_H^2 + s_{\theta_h}^2 m_S^2) \quad (2.7a)$$

$$\lambda_2 = \frac{1}{2v_2^2} (s_{\theta_h}^2 m_H^2 + c_{\theta_h}^2 m_S^2) \quad (2.7b)$$

$$\lambda_{12} = \frac{(m_S^2 - m_H^2)}{2v_1v_2} \sin 2\theta_h. \quad (2.7c)$$

The couplings of H and S to SM particles are simply given by those of the SM Higgs, scaled respectively by $\cos \theta_h$ and $\sin \theta_h$. The extension of the scalar potential results in modified expressions for the scalar self-couplings. The triple scalar self-coupling coefficients for H and S , denoted respectively by g_H and g_S , are given by

$$g_H = \frac{m_H^2}{2v_1v_2} (v_2c_{\theta_h}^3 - v_1s_{\theta_h}^3) \quad (2.8a)$$

$$g_S = \frac{m_S^2}{2v_1v_2} (v_1c_{\theta_h}^3 + v_2s_{\theta_h}^3). \quad (2.8b)$$

Furthermore, scalar mixing gives rise to additional interaction vertices between the two scalars, H - H - S and H - S - S , with respective coupling strengths

$$\mu = \frac{\sin 2\theta_h}{2v_1v_2} (v_1s_{\theta_h} + v_2c_{\theta_h}) \left(m_H^2 + \frac{m_S^2}{2} \right) \quad (2.9)$$

$$\eta = \frac{\sin 2\theta_h}{2v_1v_2} (-v_1c_{\theta_h} + v_2s_{\theta_h}) \left(m_S^2 + \frac{m_H^2}{2} \right). \quad (2.10)$$

The triple scalar interaction terms, both self-interactions and mixed scalar interactions are summarized in the following Lagrangian:

$$-\mathcal{L} \supset g_H H^3 + g_S S^3 + \mu H^2 S + \eta H S^2. \quad (2.11)$$

Returning to the interaction term which describes the dark sector of the model, as given in eq. 2.2, as S acquires a vev, one generically obtains two Majorana mass states,

$$\chi_1 = \begin{pmatrix} \psi_L \\ \psi_L^c \end{pmatrix}, \quad \chi_2 = \begin{pmatrix} \psi_R^c \\ \psi_R \end{pmatrix}$$

with masses $m_1 = g_L v_2$ and $m_2 = g_R v_2$. In this analysis the degenerate case is considered, in which the left and right couplings are related by $g_L = -g_R \equiv g$. This represents the simplest extension of this scalar extension to a dark matter scenario, giving a single dark matter candidate; the more general model described by an extended parameter space is left for future study. In the case of two mass-degenerate Majorana states, one can equivalently describe the picture in terms of a single Dirac fermion, $\chi = (\xi \quad \eta^c)^T$, where

$$\xi = \frac{1}{\sqrt{2}} (\psi_L + i\psi_R^c) \quad \eta = \frac{1}{\sqrt{2}} (\psi_L - i\psi_R^c),$$

with mass $m_\chi = g v_2$. The dark sector is then described by

$$\bar{\chi}(i\not{\partial} - m_\chi)\chi - \frac{m_\chi}{v_2} h_2 \bar{\chi}\chi. \quad (2.12)$$

With the addition of the dark matter mass, the model is then completely described by the set of four parameters,

$$\{v_2, m_S, \theta_h, m_\chi\}.$$

3 New Decay Channels

3.1 Partial Widths

A dark matter candidate that couples to the Higgs introduces a new contribution to the Higgs invisible width, Γ_{inv} . The associated experimental signature is a channel resulting in missing energy, denoted \cancel{E}_T . For $m_\chi < m_H/2$, the channel $H \rightarrow \chi\bar{\chi}$ gives a contribution

$$\Gamma_{\text{inv}} = \frac{s_{\theta_h}^2 m_H}{8\pi} \left(\frac{m_\chi}{v_2} \right)^2 \left(1 - \frac{4m_\chi^2}{m_H^2} \right)^{3/2}. \quad (3.1)$$

Moreover, additional non-SM decay modes arise from the scalar mixing terms. The total Higgs width receives new contributions from the decay to an S pair. If S is sufficiently light, the decay $H \rightarrow SS$ is kinematically allowed, with a partial width given by

$$\Gamma_{HSS} = \frac{\eta^2}{8\pi m_H} \left(1 - \frac{4m_S^2}{m_H^2} \right)^{1/2}. \quad (3.2)$$

In light of experimental exclusion limits on a light Higgs, perhaps the other mass regions are the more interesting cases — that is either the case in which $m_S \sim m_H$, or the scenario in which the new scalar is much heavier and has not yet been discovered at the energies currently probed by colliders. If S is very heavy, the dominant new scalar decay mode is its decay to an H pair; the expression for the width is analogous to eq. 3.2 upon the exchanges $m_H \leftrightarrow m_S$ and $\eta \rightarrow \mu$. For the intermediate regions, one may consider the three-body decays to one real and one virtual scalar, with the latter decaying to a fermion pair. More specifically, for the case in which $m_H/2 < m_S < m_H$, the accessible decay is $H \rightarrow SS^* \rightarrow S f \bar{f}$, where f may be any SM fermion (excluding the top quark), or χ , if the

Scalar mass hierarchy	Accessible decay modes
$m_S < m_H/2$	$H \rightarrow SS$
$m_H/2 < m_S < m_H$	$H \rightarrow Sf\bar{f}$
$m_H < m_S < 2m_H$	$S \rightarrow Hf\bar{f}$
$2m_H < m_S$	$S \rightarrow HH$

Table 1: Summary of the available scalar-to-scalar decay modes for various regions of the additional scalar mass, m_S , relative to the SM Higgs mass. It is implicit that for each case the invisible decay to $\chi\bar{\chi}$ is included for each scalar if its mass is greater than $2m_\chi$. For the intermediate mass ranges, f may denote either a SM fermion, or χ , if kinematically permitted.

DM is sufficiently light. The expressions for the relevant three-body widths (distinguishing between f_{SM} and χ) are given by the following:

$$\Gamma(H \rightarrow Sf\bar{f}) = \frac{s_{\theta_h}^2 \eta^2}{8\pi^3} \frac{m_S^2}{m_H^3} \left(\frac{m_f}{v_1} \right)^2 I(2m_f/m_S, m_H/m_S), \quad (3.3a)$$

$$\Gamma(H \rightarrow S\chi\bar{\chi}) = \frac{c_{\theta_h}^2 \eta^2}{8\pi^3} \frac{m_S^2}{m_H^3} \left(\frac{m_\chi}{v_2} \right)^2 I(2m_\chi/m_S, m_H/m_S). \quad (3.3b)$$

Here

$$I(y, z) = \int_1^{x_{max}} dx \frac{\sqrt{x^2 - 1}}{(z - 2x)^2} \frac{(1 + z^2 - y^2 - 2zx)^{3/2}}{(1 + z^2 - 2zx)^{1/2}}, \quad (3.3c)$$

where $x_{max} = (1 + z^2 - y^2)/(2z)$. The y term is neglected for $y = 2m_f/m_S$. As would be expected, the expressions for the intermediate case with S heavier than H are obtained by exchanging $m_H \leftrightarrow m_S$, $\eta \rightarrow \mu$, and $s_{\theta_h} \leftrightarrow c_{\theta_h}$. The mass regions and accessible decay channels are summarized in table 1.

3.2 Scalar Couplings

The interaction vertices between H and S , arising from the mixed cubic terms in the scalar potential, provide possibly significant new contributions to decay widths and production processes.¹ It can be seen from eqs. 2.9 and 2.10 that these couplings may become large for certain values of the mass and vev of the additional scalar. Physical quantities which would otherwise be suppressed — either by a small mixing angle or by nature of being a higher order effect — may be non-negligible. Figures 1 and 2 show the dependence of the scalar couplings, μ and η respectively, on the scalar parameters.

3.3 Three-Body Decays

One typically expects the contribution of the three-body widths to be subdominant, due to suppression by the phase space integration. As previously noted, for certain regions

¹The contribution of this vertex to Higgs production at a linear collider will be further discussed in section 5.1

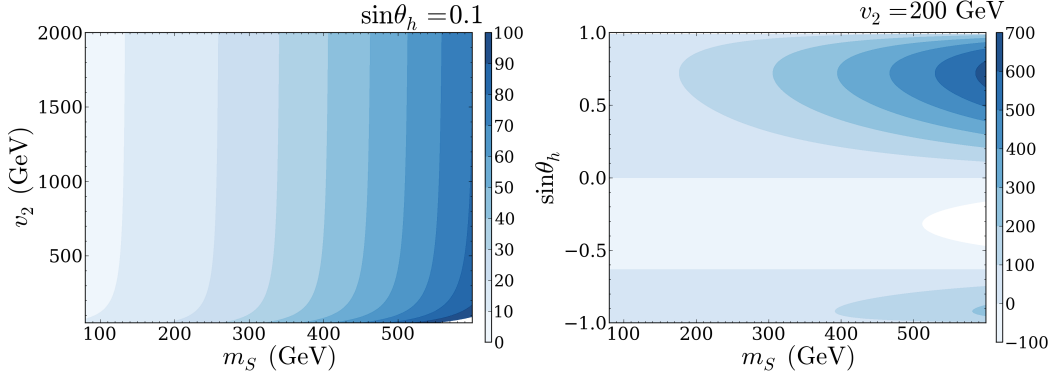


Figure 1: Value of the H - H - S coupling constant, μ , over various regions of scalar parameter space. The left figure gives the dependence in (m_S, v_2) space for a discrete value of the mixing angle, while the right shows the dependence over (m_S, s_{θ_h}) space for chosen value of v_2 .

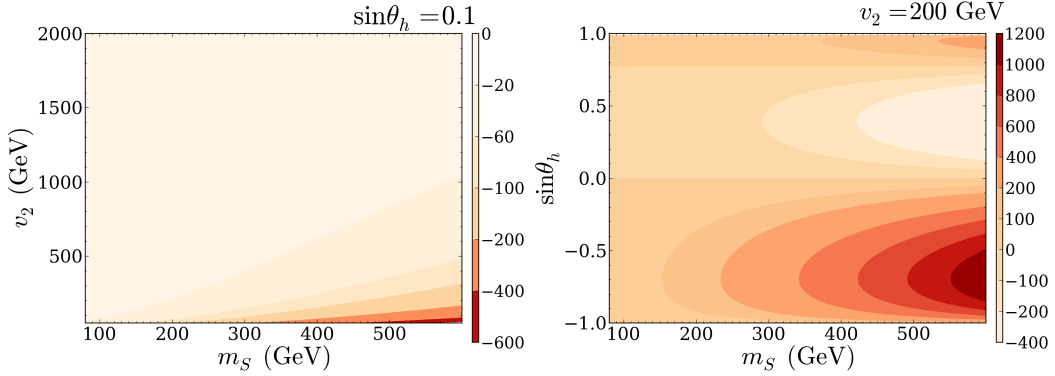


Figure 2: Dependence of H - S - S coupling, η , on the scalar parameter space. The description of subfigures is as given in figure 1.

of parameter space, the tri-scalar couplings may be large enough to partially offset these effects. In the intermediate mass regions, where the three-body decays are kinematically relevant, the magnitudes of these couplings grow very large only for extremal values of the mixing angle or the scalar vev, however it warrants further consideration to verify that the three-body decay widths remain subdominant, and may be neglected. A more detailed exploration of the relative size of the three-body contribution is presented in the following. The partial width of the three-body decay is calculated and compared with the more dominant contributions.

The mass regions of interest relevant for the three-body decays of H and S are the two intermediate ranges — that is, $m_H/2 < m_S < m_H$ and $m_H < m_S < 2m_H$. The different choices of final-state fermion pair — either a SM fermion, or χ — are presented separately. The decay $H(S)$ to $S(H)$ and a SM fermion pair is shown in figure 3. In this case, the

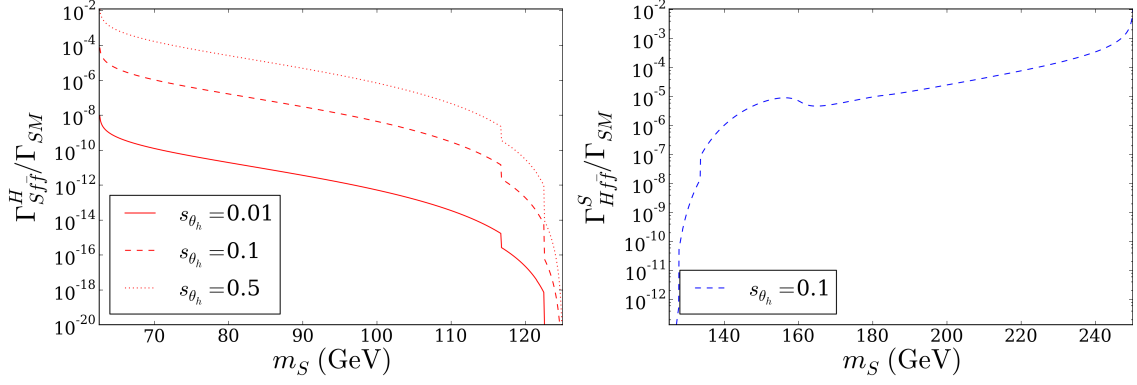


Figure 3: Relative magnitude of the three-body decay widths to a scalar and SM fermion pair. A simplified branching ratio is shown, taken as the ratio of the three-body width to the total visible width. The width $H \rightarrow S f \bar{f}$ is shown in the left figure, and $S \rightarrow H f \bar{f}$ on the right. In both cases, the scalar vev is fixed to be $v_2 = 200$ GeV, and the mixing angle is varied discretely.

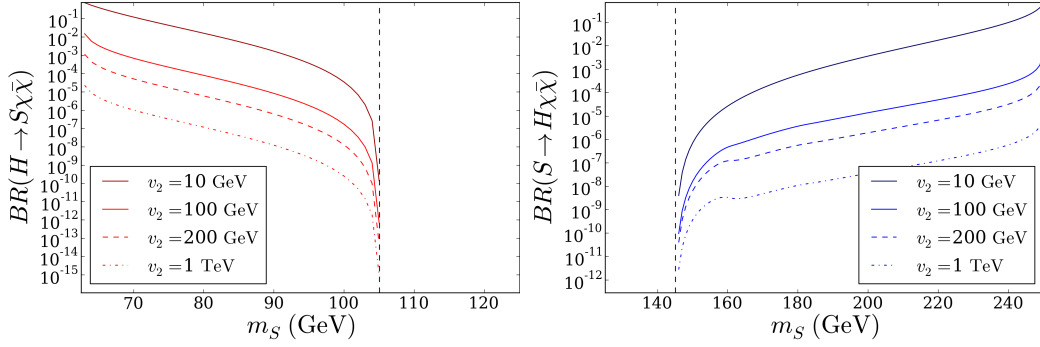


Figure 4: Branching ratio for the three-body decays to a scalar and dark matter pair. The dark matter mass is fixed at $m_\chi = 10$ GeV, and the scalar mixing angle is set to $\sin \theta_h = 0.5$. Branching ratios for $H \rightarrow S \chi \bar{\chi}$ and $S \rightarrow H \chi \bar{\chi}$ are shown in the left and right figures respectively.

reference point for comparison is chosen to be the total width for decay to SM particles,

$$\Gamma_{SM}^H = c_{\theta_h}^2 \Gamma_h^{SM}(m_H) \quad (3.4)$$

$$\Gamma_{SM}^S = s_{\theta_h}^2 \Gamma_h^{SM}(m_S), \quad (3.5)$$

i.e., the total Higgs width under the SM, scaled by the appropriate factor of the mixing angle. This effectively gives the branching ratio under a few simplifications. The other new contributions to the total width are the two body decays to a scalar pair, which is kinematically forbidden in the intermediate mass regions, and to $\chi \bar{\chi}$, which is neglected for

simplicity; the inclusion of the invisible decay to the total width would simply result in a further overall reduction of the branching ratio. The result is presented as a function of m_S , discretely varying the mixing angle. It can be seen in figures 1 and 2, that over the intermediate mass intervals, both couplings μ and η show little dependence on the scalar vev, except for a small increase towards very small values of v_2 . Hence, its value is fixed to $v_2 = 200$ GeV. Several values of $\sin \theta_h$ are shown for the H decay width, given in the left figure. Despite the non-trivial functional dependence of the coupling, the primary effect of varying the mixing angle is an overall scaling of the width, $\propto \sin^2 \theta_h$. This dependence vanishes in the case of the corresponding S decay, due to the factor of $\sin^2 \theta_h$ in the normalizing visible width, as seen in eq. 3.5. A very minimal effect was seen upon varying the mixing angle, and so only one value is shown.

When considering the analogous decay to χ rather than a SM fermion, the dark matter mass enters into the three-body width; the invisible decay is thus included in the analysis as the parameter space is already extended. The normalizing quantity is chosen as the total width, giving the branching ratio for $H(S) \rightarrow S(H)\chi\bar{\chi}$. The results are shown in figure 4. In the given result, the value of m_χ was chosen to be 10 GeV. The primary influence of the χ mass on the magnitude of the three-body width is through its contribution to the coupling, through the ratio m_χ/v_2 , and results primarily in an overall scaling. For most of the scalar mass range of interest however, the values of the dark matter mass for which the relevant decays are kinematically permitted, are at most of order ~ 10 GeV, i.e. $m_\chi \lesssim 50$ GeV. Hence, as the order of m_χ does not change drastically in comparison to the variation of the scalar vev, its value is fixed such that it is near the larger end of the allowed range, and the three-body decays of both H and S are allowed over most of the m_S range considered. In keeping with the aim of investigating the possible extremal values of these partial widths, a further simplification is made with respect to the mixing angle. The most apparent effect of the mixing angle on the overall magnitude is an overall scaling by $\sim \sin \theta_h$; therefore it is set to roughly what will be later shown to be the maximum value allowed by experimental constraints, with $\sin \theta_h = 0.5$.

Over most of parameter space, the three-body contributions to the H and S widths are considerably small; except for large values of the mixing angle or small values of the vev, and values of $m_S \simeq m_H/2$ or $\simeq 2m_H$, in most cases $BR \lesssim 10^{-4}$. For most parameter values, one is justified in neglecting these contributions in calculating the total width. In the case of the decay involving a $\chi\bar{\chi}$ pair, the branching ratio does become more significant for very small values of the new scalar vev, i.e. $\mathcal{O}(10)$ GeV, or more specifically, when $v_2 \sim m_\chi$. However, as will be discussed later, such small values of v_2 are disfavoured by other experimental and theoretical limits, and the remaining analysis focuses on vevs of order 100 GeV and larger, neglecting these three-body contributions. The couplings μ and η do assume larger values for regions of parameter space over which the three-body decays are relevant, but they only become very large (i.e. orders of magnitude larger) in regions where these decays are kinematically forbidden, and the quantity of interest is not the total widths. This may have relevance towards off-shell scalar production processes, a topic which will be further discussed in later sections.

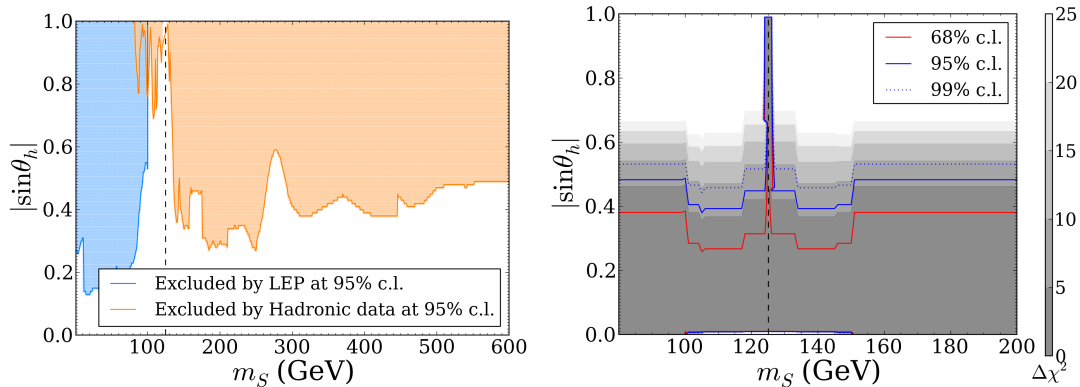


Figure 5: Limits on scalar parameter space, $(m_S, |\sin \theta_h|)$ from current collider data. Left: Regions excluded by LEP and Tevatron/LHC Higgs exclusion searches, at 95% c.l. Right: Preferred regions compatible with measured LHC Higgs signal strength. The regions allowed at 68%, 95%, and 99% c.l. are shown.

4 LHC Limits

Current LHC Higgs data have been found to be consistent with the SM Higgs sector. Such a result places limits on a scalar extension, both with respect to the modification of production cross sections of the SM-like Higgs, as well as the fact that a second scalar has evaded discovery as yet. This scenario, in which a new scalar has escaped detection by hadron colliders at the currently achieved energies and luminosities, generally constrains either the mixing parameter to be small or the scalar mass to be heavy. The limits posed by LHC Higgs data are reviewed here, and limits resulting from new contributions to the Higgs widths are determined.

4.1 Higgs Signal Strength and Exclusion Searches

In the following section, the compatibility of a mixed two-Higgs scenario with current hadronic collider data is reviewed. The scalar parameter space is strictly constrained by Higgs searches, with respect to both past exclusion searches, and measured signals, particularly in light of the recent Higgs discovery. The precise limits on a scalar singlet extension posed by LHC Higgs data have been determined by ref. [1]. Since publication of this work, updated LHC Higgs results have been released, as well as a version of the publicly available code used throughout the analysis, which incorporates these new data. There is also a slight distinction from the present analysis, in the convention chosen to define the mass eigenstates, as well as the inclusion here of the nonzero $H \rightarrow SS$ and $S \rightarrow HH$ branching ratios.² In light of this, the limits are reproduced here for completion, under these modifications, following the procedure of [1].³ The publicly available code HIGGSBOUNDsv4.3.1 [21–25]

²Ref. [1] takes the scalar defined by $c_{\theta_h} h_1 - s_{\theta_h} h_2$ to be the lighter of the two, rather than fixing it to be the 125 GeV boson, as is done here, effectively switching $\sin \theta_h \rightarrow \cos \theta_h$, for $m_S < 125$ GeV.

³Ref. [4] conducts a similar analysis, using an alternative approach to the signal strength limit.

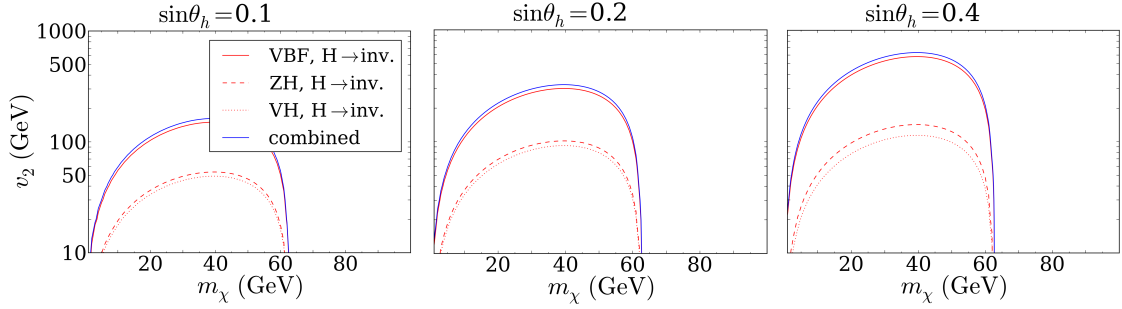


Figure 6: Limits on (m_χ, v_2) parameter space, from ATLAS upper bounds on signal strength in Higgs invisible decays, for discrete values of the mixing angle, below the upper bound set in section 4.1. The regions below the curves are excluded at 95% c.l.

is used to determine the limiting region in the space defined by the scalar mass and mixing angle, by exclusion from LEP, Tevatron and LHC data. In particular, LEP searches from refs. [26–36] are used, and experimental LHC/Tevatron results are those in refs. [37–84], with more recent LHC results from Refs. [85–90]. The region allowed at 95% c.l. is shown in figure 5, with regions excluded by LEP and Tevatron/LHC presented separately.

While the limits posed by exclusion searches constrain the model in the absence of a signal, the recent Higgs discovery necessitates the complementary limits from compatibility with this observed signal. Results are determined using HIGGSIGNALSV1.4.0 [91, 92]. The experimental results used to obtain the constraints are given in refs. [93–104]. For light scalars, $m_S < 80$ GeV, the strictest limit is found by LEP exclusion, giving an upper bound of $|\sin \theta_h| \lesssim 0.15$, while the upper limit from LHC exclusion searches is between $|\sin \theta_h| \lesssim 0.3$ at its most stringent, in the region $m_S \sim 170$ –250 GeV, and is as large as 0.4–0.6 for higher masses. The constraint posed by the measured signal strength in Higgs production at LHC, which places an upper bound (at 95% c.l.) on the mixing angle of $|\sin \theta_h| \lesssim 0.5$, for scalar masses $m_S < 100$ GeV or $m_S > 150$ GeV, and $|\sin \theta_h| \lesssim 0.4$ for scalar masses within a 25 GeV window of 125 GeV. When m_S approaches m_H , within the detector mass resolution, this represents the degenerate limit which simply reproduces the SM signal — in other words, the signal strength for a 125 GeV scalar with SM couplings scaled by $\cos^2 \theta_h + \sin^2 \theta_h = 1$ — hence the mixing angle is unconstrained in this narrow region. Figure 5 shows the regions preferred by LHC Higgs signal compatibility.

Additional limits arise from electroweak precision data (EWPD), and theoretical constraints such as perturbativity and renormalization group (RG) evolution of the couplings, which may tighten the mixing angle upper bound, to $|\sin \theta_h| \lesssim 0.3$ in the heavier S region — $m_S \gtrsim 600$ GeV [1]. Such considerations also place further lower bounds on the S vev in some cases, again disfavouring small v_2 ; the restrictions were not in conflict with any of the present results. Similar analyses in refs. [4, 5] also include such theoretical considerations, obtaining similar bounds.

4.2 Invisible Signals

The extension to the SM scalar sector results in a strict constraint posed by Higgs production searches and measurements, due to scaling of Higgs couplings to SM particles and the allowed mass of a new Higgs-like scalar; the allowed values of the scalar parameters are described in the previous subsection. The remaining parameter — the dark matter mass — becomes significant when focusing on searches with invisible signatures. A direct limit on the dark matter mass, as well as the additional scalar vev, is found in Higgs production with subsequent invisible decay channels.

A recent ATLAS search [105] for invisible Higgs decays, in both vector boson fusion (VBF), and associated vector boson production modes, gives an upper limit on the Higgs invisible branching ratio. ATLAS obtains limits from three production channels — vector boson fusion, associated Z production with subsequent leptonic Z decays, and associated vector boson, V (W or Z), with hadronic W/Z decay, as well the combined limit from the three. The search corresponds to 4.7 fb^{-1} of data at centre of mass energy 7 TeV, and 20.3 fb^{-1} at 8 TeV. Upper limits are given at 95% c.l. on the production cross section times invisible branching ratio signal strength. This signal strength, denoted here by ζ is simply the production cross section times branching ratio, normalized by the SM production cross section

$$\zeta = \frac{\sigma}{\sigma_{SM}} \times \mathcal{B}(h \rightarrow \text{inv}). \quad (4.1)$$

More specifically, for H , this becomes

$$\zeta_H = c_{\theta_h}^2 \frac{\Gamma_{\text{inv}}}{\Gamma_{\text{tot}}} = \frac{c_{\theta_h}^2 s_{\theta_h}^2 \Gamma_{\text{inv}}}{c_{\theta_h}^2 \Gamma_{SM} + s_{\theta_h}^2 \Gamma_{\text{inv}}}. \quad (4.2)$$

Here, $\Gamma_{\text{inv}}(m_\chi, v_2)$ is as given in eq. 3.1, with the factor s_{θ_h} written explicitly. The corresponding observable for S production and decay is obtained under exchange $m_H \rightarrow m_S$ and $s_{\theta_h} \leftrightarrow c_{\theta_h}$.

ATLAS sets upper limits on the normalized signal strength of 0.28, 0.75, and 0.78 in the VBF, leptonic ZH , and hadronic VH channels, with a combined limit of 0.25. The resulting bound on (m_χ, v_2) is given in figure 6. The 95% c.l. exclusion is shown, using the individual channels, as well the combined results. The mixing angle is varied discretely, with values below the upper limit obtained in section 4.1. The constraint represents the experimental bound to the invisible H width, at mass 125 GeV. A similar search by CMS [41] gives an upper bound on the invisible branching ratio as a function of Higgs mass, although the limit at $m_H = 125 \text{ GeV}$ is looser than that given by ref. [105]. As this gives a bound for a general scalar mass, this is applied to the invisible S width. For mixing angle values which remain consistent with the Higgs production signal strength however, the corresponding limit applied to the invisible branching ratio of S does not significantly constrain the parameter space.

4.3 Total Higgs Width

An analysis by CMS obtains a limit on the width of the Higgs boson, by a method which uses the ratio between on-shell and off-shell cross section measurements [106]. CMS obtains

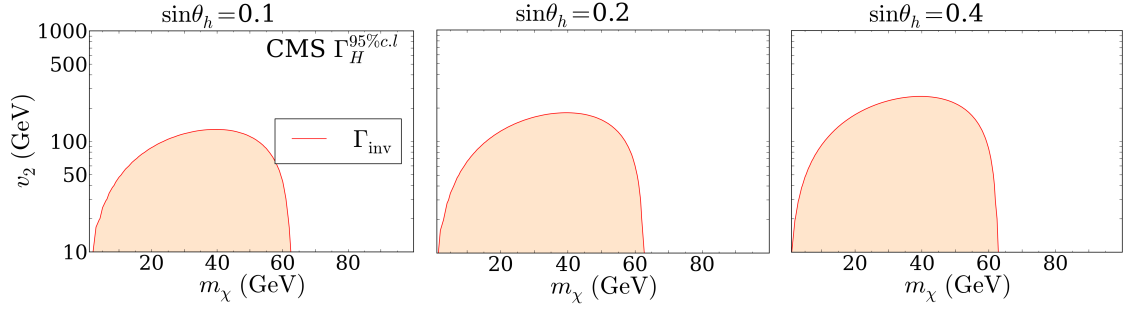


Figure 7: Limit on dark matter parameters resulting from invisible contribution to total Higgs width. Results are obtained using the CMS upper bound on the total Higgs width, assuming the absence of additional two-body scalar decays, i.e. in the heavy S regime. The shaded regions are excluded at 95% c.l.

an upper limit on the total Higgs width of 26 MeV, at 95% c.l. For most of the scalar mass range, this provides an additional constraint on the dark matter mass and coupling; if $m_S > m_H/2 \sim 63$ GeV, the decay of H to an S pair is kinematically forbidden, and as seen in section 3.3, the three-body contributions are negligible. Assuming that the only non-SM contribution to the Higgs width is the invisible decay $H \rightarrow \chi\bar{\chi}$, the resulting limit on the dark matter mass and scalar vev is given in figure 7. The constraint posed by measured invisible decays however, gives the stricter limit.

In the light S regime — that is, in the subregion of parameter space for which $m_S < m_H/2$ — the total width also receives a contribution from the decay channel $H \rightarrow SS$. This provides additional direct experimental sensitivity on the allowed values of the scalar vev, as it enters into the mixed scalar coupling, which depends additionally on the mixing angle and scalar mass. Each of these three parameters, $(\sin\theta_h, v_2, m_S)$, is varied discretely in turn, giving the exclusion region in the other two. The results are given in figure 8. Both the case for which the scalar decay channel is the only new contribution (which is the case for heavy dark matter), as well as that for which both scalar and invisible decays are present. In the latter case, m_χ is chosen such that the invisible contribution is below the upper bound over most of the v_2 range considered, as shown in figures 6 and 7; the value is taken to be $m_\chi = 10$ GeV.

The resulting exclusion regions in figure 8 show the extremal allowed values of the mixing angle and scalar vev, which are more or less proportionate as each is varied. The figures in the top row show a lower bound on v_2 , which increases with the mixing angle, and remains constant with m_S , in the kinematically allowed range. Varying v_2 discretely (shown in the middle row), one sees an upper bound on $|\sin\theta_h|$ which relaxes with increasing v_2 . The regions in (v_2, s_h) (bottom row) illustrate this behaviour. Smaller values of the scalar vev, $v_2 \lesssim 100$ GeV are disfavoured, except for very small values of the mixing angle; the allowed range of $\sin\theta_h$ is relaxed with increasing v_2 , and for $v_2 > 200$ GeV the upper bound on $\sin\theta_h$ is well above that imposed by the LHC signal strength.

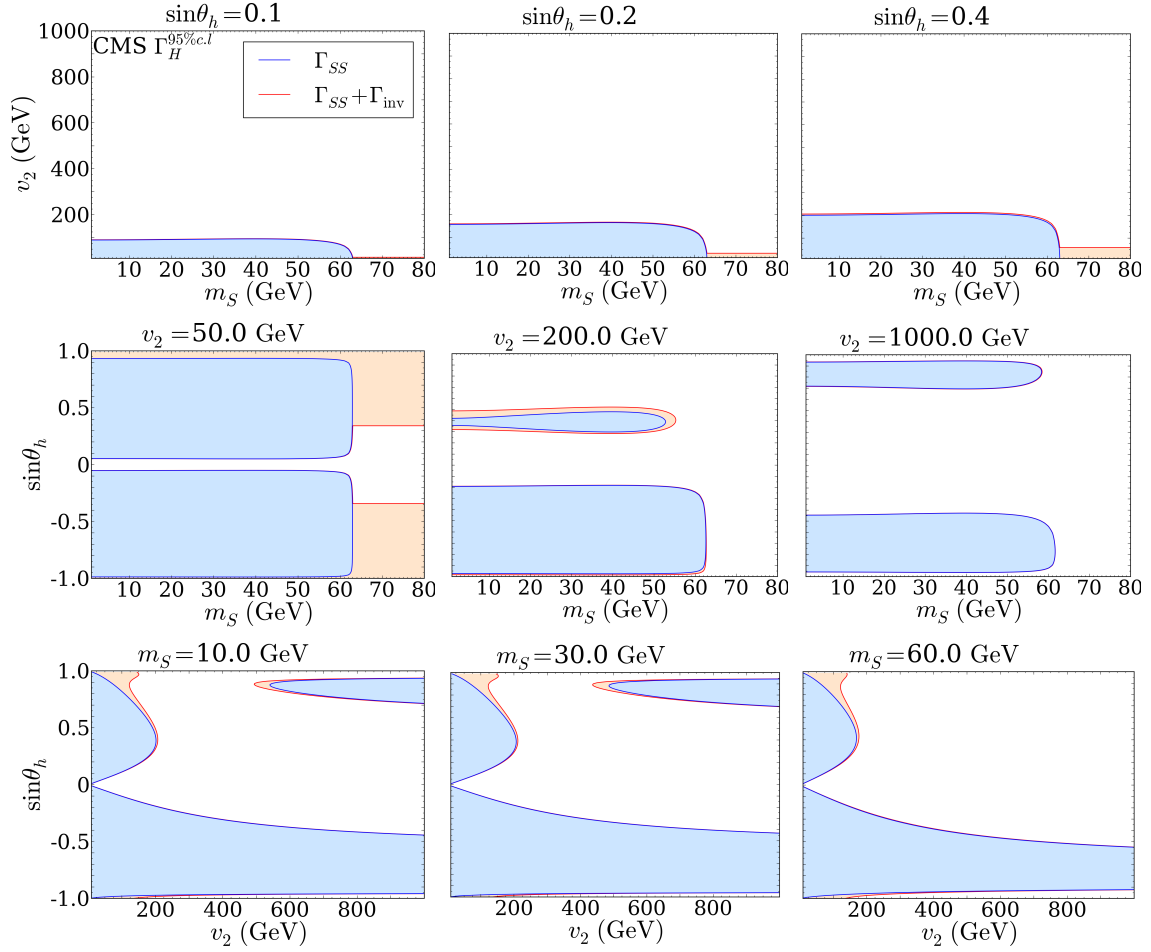


Figure 8: Limit resulting from contribution of $H \rightarrow SS$ decay to total Higgs width. The shaded regions represent the region excluded at 95% c.l. by the CMS limit. From the top row down, $\sin\theta_h$, v_2 , m_S are each varied discretely in turn. The blue curve/region corresponds to the case for which the decay to SS is the only non-SM contribution, and red to the case which also includes the invisible channel.

5 ILC Prospects

The current experimental results impose that an additional Higgs-like scalar, or any general extended Higgs sector, has evaded detection at the current collider energies. A possible next step which suggests itself, is to move toward a precision environment and search for signatures of a scalar extension, through its influence on Higgs precision measurements. In the following discussion, the potential discovery reach, and possible signatures of a mixed Higgs scenario are considered at the ILC.

By nature of being a lepton collider the ILC will offer substantially cleaner signals, and is therefore much better suited to precision measurements; such a task is not possible at the LHC due to the significant QCD background. The cleaner environment, as well as

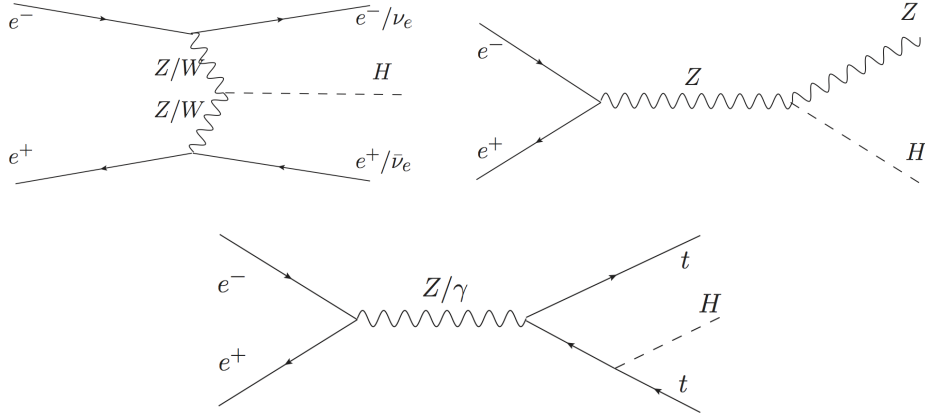


Figure 9: Feynman diagrams for leptonic Higgs production. From left to right, and top to bottom, subprocesses are: vector boson fusion (VBF), Higgs-strahlung, and for higher energies, associated top production ($t\bar{t}H$).

detectors and instrumentation associated with a lepton collider, allow for the possibility to reconstruct Higgses more cleanly and in additional decay channels. Furthermore, the capability for polarized beams adds greater sensitivity to spin effects, by allowing greater control on the initial helicity states. This is advantageous in that beam polarization provides the ability to fully characterize a process with respect to the differences in interactions and couplings between left and right-handed particles. Beam polarization is particularly important in electroweak processes, which are sensitive to spin. There are several key motivations for using polarized beams at ILC, which vary with the particular type of process under study. Firstly, oppositely polarized beams enhance luminosity in electron-positron annihilation processes, as an electron annihilates a positron of opposite helicity. Beam polarization asymmetry is also an informative variable in precision electroweak measurements, via the $e^+e^- \rightarrow f\bar{f}$ process. Another advantage is the ability to increase the signal to background ratio, in processes that occur predominantly through a specific initial helicity configuration, thereby optimizing either certain SM signals or new physics searches. In light of its proposed features and capabilities, Higgs parameters such as the top Yukawa coupling, Higgs branching ratios, couplings to vector bosons, and the Higgs self coupling (of particular focus here), are perhaps well within the reach of the ILC.

In lepton collisions, one loses the gluonic contributions that dominate LHC Higgs production, and the remaining processes are the electroweak modes. The leading modes in leptonic Higgs production are the Higgs-strahlung process, and W boson fusion. Additional contributions are present in Z boson fusion, and associated heavy quark production at higher energies. The corresponding Feynman diagrams are shown in figure 9. Diagrams correspond interchangeably to either H or S production, with the couplings scaled by the appropriate factor of the mixing angle. Naturally, the Higgs production cross section is larger in hadron collisions than in lepton collisions, due to the leading QCD processes; by experimental design the LHC optimizes Higgs production, with discovery being the priority.

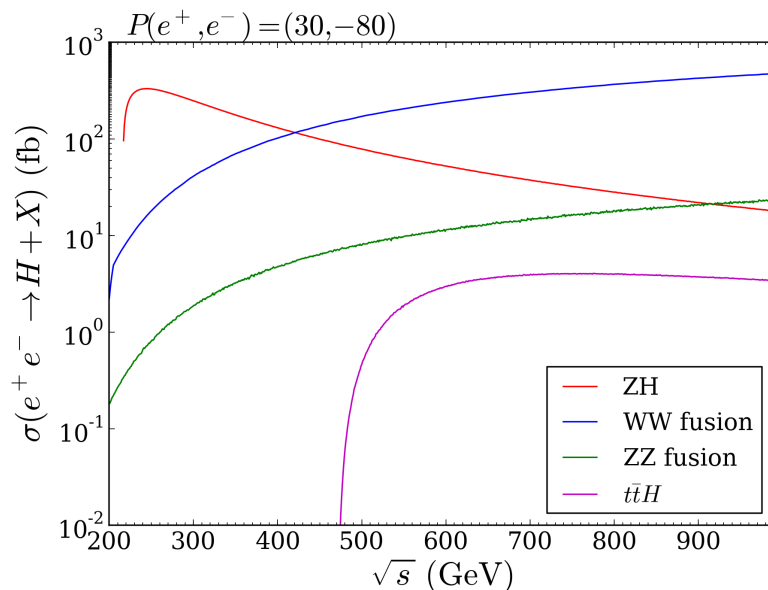


Figure 10: Leptonic Higgs production cross section as a function of centre of mass energy, for beam polarization $P(e^+, e^-) = (30, -80)$. The Higgs mass is taken to be 125 GeV.

Although production cross sections are smaller at a lepton collider, higher order effects are much less significant in the case of electroweak processes, offering greater ease of calculability and less theoretical uncertainty associated with higher order effects. Cross sections for Higgs production in e^-e^+ collisions are determined at LO, using MADGRAPH5 [107]. The cross sections as a function of centre of mass energy are shown in figure 10, for beam polarization $(P_{e^+}, P_{e^-}) = (30, -80)$. More specifically, this denotes an electron beam which is 80% left-polarized, and a positron beam that is 30% right-polarized. The formal definition of polarization is

$$P = \frac{N_R - N_L}{N_R + N_L}, \quad (5.1)$$

where N_R and N_L are the number of particles with spin parallel or antiparallel to the direction of motion. An equivalent interpretation of this number, is the percentage of events for which the helicity is known, with positive or negative signifying right or left.

A possible experimental program includes running at centre of mass energies 250 GeV, 500 GeV, and 1 TeV, with ability to obtain beam polarizations of $(P_{e^+}, P_{e^-}) = (30, -80)$ at the lower two energies, and $(20, -80)$ at 1 TeV [108]. The displayed cross sections correspond to production of the SM-like Higgs, i.e. $m_H = 125$ GeV, and omitting the mixing angle factor $\cos^2 \theta_h$.

Depending on the mass of the additional scalar, it may also be possible to observe direct production of the new particle. For each centre of mass energy, and the particular range of m_S , there are various possible modes by which the additional scalar may be observed. In addition to direct S production, the new scalar may also be observed by Higgs

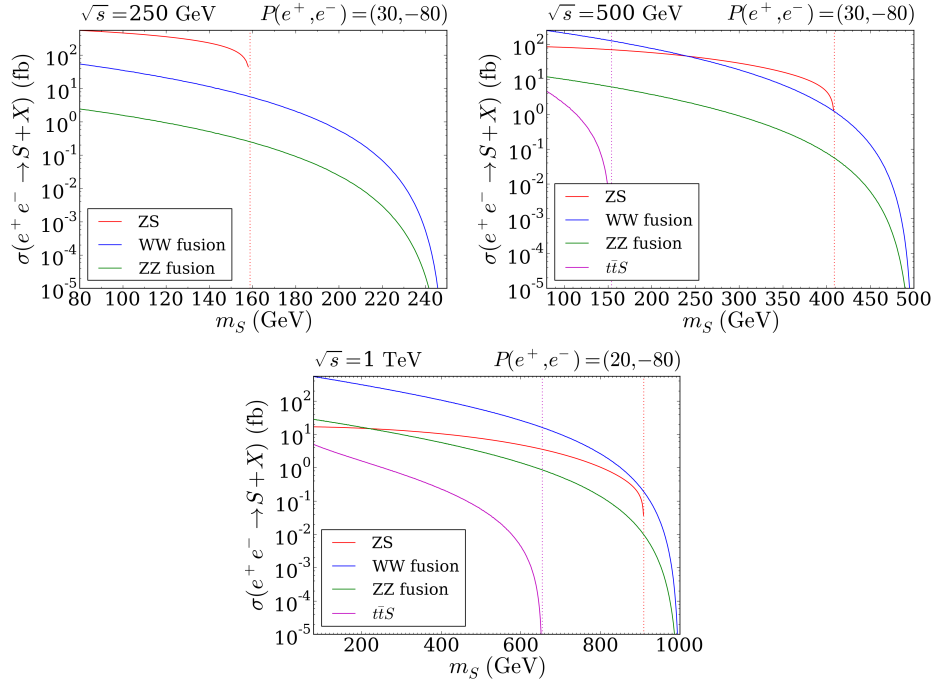


Figure 11: Higgs production cross section in electron-positron collisions, for centre of mass energies, $\sqrt{s} = 250, 500$ GeV, and 1 TeV. Cross sections are given at leading order, for electron polarization -80 , and positron polarization 30 for 250 and 500 GeV, and 20 for 1 TeV.

production and subsequent decay to a scalar pair — for the light S case — or through double scalar production processes. Cross sections for single S production are presented in Figure 11 as a function of S mass, for proposed operational energies of the ILC and respective beam polarizations corresponding to each centre of mass energy. Maintaining convention, S production cross sections have been normalized by the mixing factor, omitting the scaling by $\sin^2 \theta_h$ in this figure.

An important feature of the ILC is the sensitivity to processes in which two Higgs (or two scalars) are produced. Such processes could be a distinguishing signature of a mixed Higgs model, and would allow the possibility to probe scalar parameters which are uniquely modified, an effect which is not measurable at the LHC. In the following section, the potential observation of the di-Higgs processes is further explored.

5.1 Di-Higgs Processes

It is interesting to note that the potentially large couplings of the trilinear scalar terms, and modification to the SM value of the Higgs self-couplings, could result in distinguishing effects in measurements of the double Higgs processes. Precision measurements required to probe the Higgs self-couplings and other parameters of the scalar potential, are beyond the scope of current hadron colliders; such measurements fall under the domain of the ILC. The scalar interaction vertices give rise to double scalar production processes which may

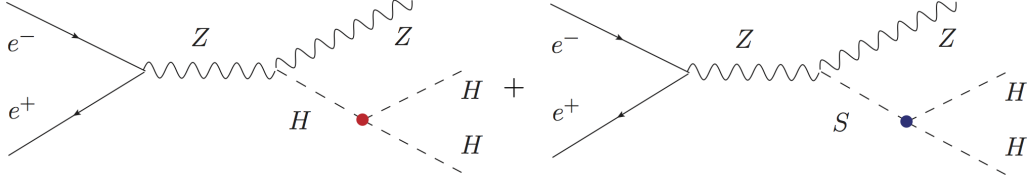


Figure 12: Diagrams showing contribution of Higgs self coupling (left) and mixed scalar coupling (right) to di-Higgs production.

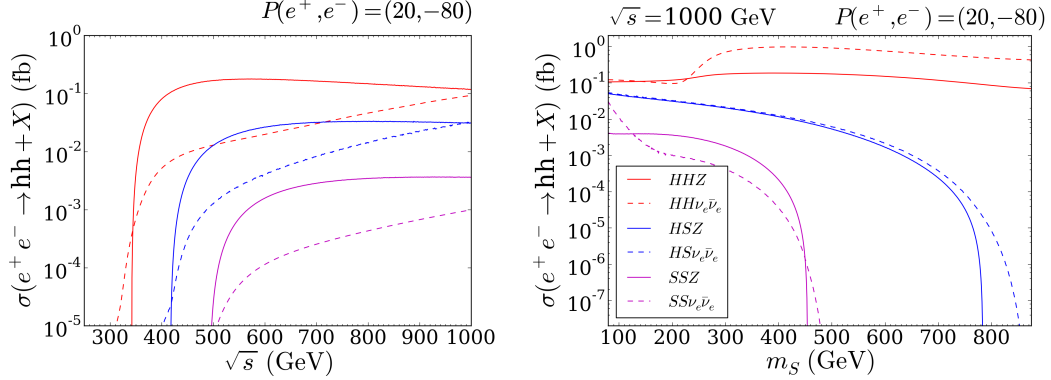


Figure 13: Cross sections for scalar pair production processes, presented both as a function of centre of mass energy (left) and scalar mass, m_S , at $\sqrt{s} = 1$ TeV (right). In the former case, the scalar mass and vev are both taken to be 200 GeV, and the mixing angle is fixed at $s_{\theta_h} = 0.4$.

produce H , S , or H - S pairs. The following will focus on measurement of the double Higgs (H pair) process.

An example Feynman diagram for di-Higgs production is given in figure 12, showing the contributions of the self-coupling and mixed scalar coupling, to the double Higgs-strahlung process. Additional diagrams contributing to this process are given in appendix A. These are referred to as ‘background’ subprocesses, in the sense that the contributions are not proportional to either the self-coupling, or mixed scalar coupling. These contributions arise from the Higgs-vector boson interactions. Hence, the dependence of the di-Higgs cross section on these scalar couplings is not straightforward; translating measurement of the cross section to a measurement of either one of the couplings is therefore more complex than in the SM case. For this reason, the quantitative effect on measurement of the cross section is analyzed, rather than that of the self-coupling. At higher energies, approaching 1 TeV, the W fusion mode becomes more significant. Analogous diagrams exist for double Higgs production in this channel, which are also given in appendix A.

Under this model, the cross section for di-Higgs production differs from the SM value in several aspects:

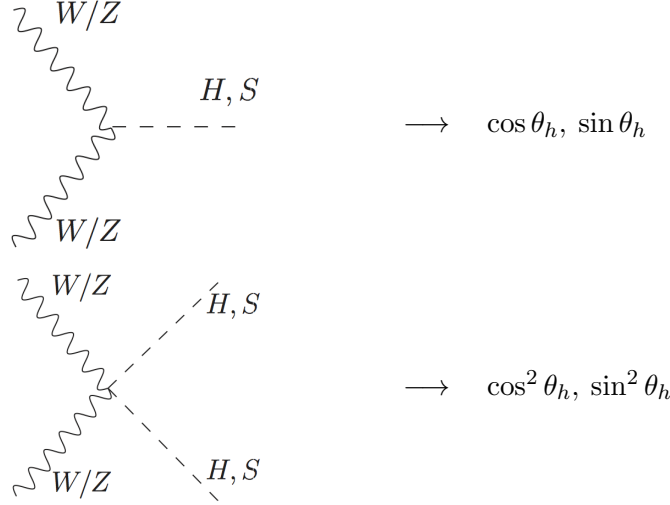
- the triple Higgs self-coupling is modified, according to

$$\frac{m_H^2}{2v_1} \rightarrow \frac{m_H^2}{2v_1 v_2} (v_2 c_{\theta_h}^3 - v_1 s_{\theta_h}^3)$$

- the additional contribution from the mixed trilinear scalar vertex, proportional to

$$\mu = \frac{\sin 2\theta_h}{2v_1 v_2} (v_1 s_{\theta_h} + v_2 c_{\theta_h}) \left(m_H^2 + \frac{m_S^2}{2} \right)$$

- scaling by various factors of $\cos \theta_h$ and $\sin \theta_h$ in the Higgs' couplings to vector bosons



The cross section for the di-Higgs process is given in figure 13, including also the H - S , and double S processes, showing both the HHZ and $HH\nu_e\bar{\nu}_e$ production channels. The dependence on both the centre of mass energy, and the S mass is shown. In both cases, the mixing angle is fixed near its maximal allowed value, $\sin \theta_h = 0.4$, and in the latter case the S mass and vev are set to $m_S = 200$ GeV and $v_2 = 200$ GeV. Cross sections are calculated using MADGRAPH5, and the model as described in section 2 is implemented via FEYNRULESV2.0 [109].

The expected precision in measurement of the cross section for di-Higgs production has been determined by ILC projections obtained by full detector simulations of SM processes. The technical design report gives an expected precision of $\Delta\sigma/\sigma = 0.27$ for the HHZ process [110], and $\Delta\sigma/\sigma = 0.23$ for the $HH\nu_e\bar{\nu}_e$ is obtained in ref. [111]. The fractional change in the di-Higgs production cross sections for both the HHZ and $HH\nu_e\bar{\nu}_e$ processes is determined, and the parameter regions over which the effect of the mixed scalar model would be measurable is established. The fractional change in cross section, compared with the SM value, for both the HHZ and $HH\nu_e\bar{\nu}_e$ processes is calculated and plotted over the remaining scalar parameter space, allowed by existing LHC constraints. Specifically, the quantity

$$\frac{|\sigma(m_S, \sin \theta_h, v_2) - \sigma_{SM}|}{\sigma_{SM}} \quad (5.2)$$

is determined.

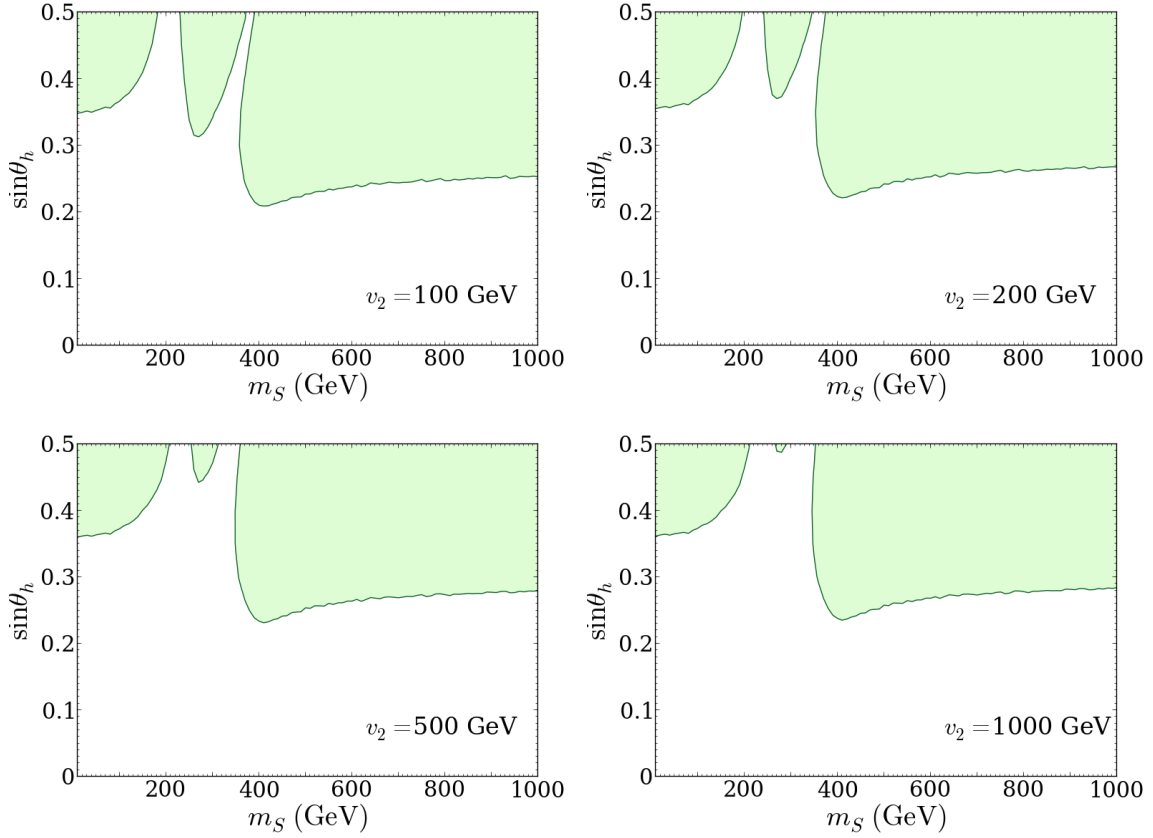


Figure 14: Measurable region in $(m_S, \sin \theta_h)$ space, based on fractional change in the HHZ production cross section, using expected ILC precision in $\Delta\sigma/\sigma$. Value of v_2 is varied discretely, as indicated. Cross sections are calculated at 500 GeV, and $(P_{e^-}, P_{e^+}) = (-80, 30)$.

The region over which the effect of the scalar mixing is within the expected ILC precision of the measurement is presented, showing the region of scalar parameter space which is within the reach of measurement via di-Higgs production. Results are presented in figures 14 and 15, in the HHZ and $HH\nu_e\bar{\nu}_e$ channels respectively. The strongest dependence is found to be in $(m_S, \sin \theta_h)$, while varying the value of v_2 has a minimal effect on the bounds of the measurable region. Cross sections are calculated for HHZ production at $\sqrt{s} = 500$ GeV and $(P_{e^-}, P_{e^+}) = (-80, 30)$, and for $HH\nu_e\bar{\nu}_e$ at $\sqrt{s} = 1$ TeV and $(P_{e^-}, P_{e^+}) = (-80, 20)$ — consistent with the values corresponding to the expected precision in the cross section measurements. The greatest change in the cross section is found to be for larger values of m_S , due to the exchanged S going on shell and decaying to an HH pair, in the contribution $\propto \mu$. For light S , there is still a possible measurable effect for $\sin \theta_h > 0.25 - 0.4$ that is within the region allowed by existing LHC constraints.

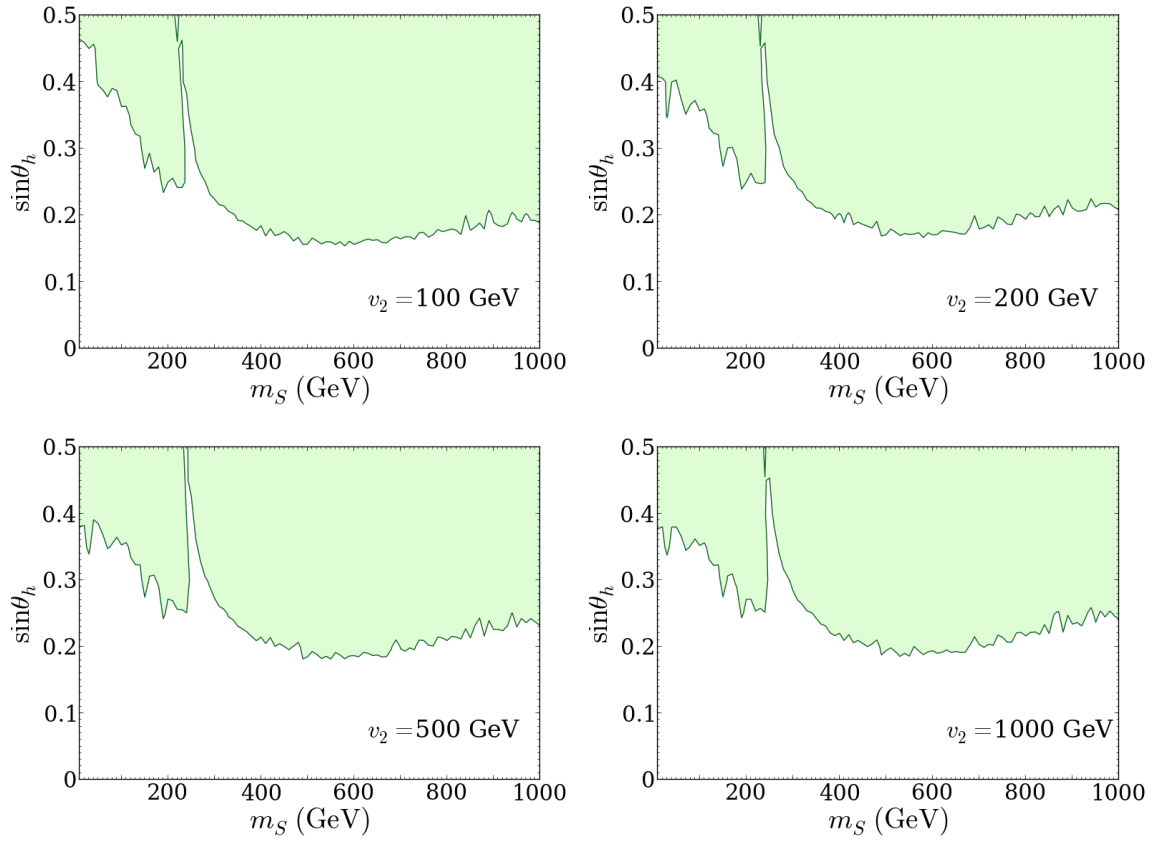


Figure 15: Measurable region in $(m_S, \sin \theta_h)$ space, based on fractional change in the $HH\nu_e\bar{\nu}_e$ production cross section, using expected ILC precision in $\Delta\sigma/\sigma$. Value of v_2 is varied discretely, as indicated. Cross sections are calculated at 1 TeV, and $(P_{e-}, P_{e+}) = (-80, 20)$.

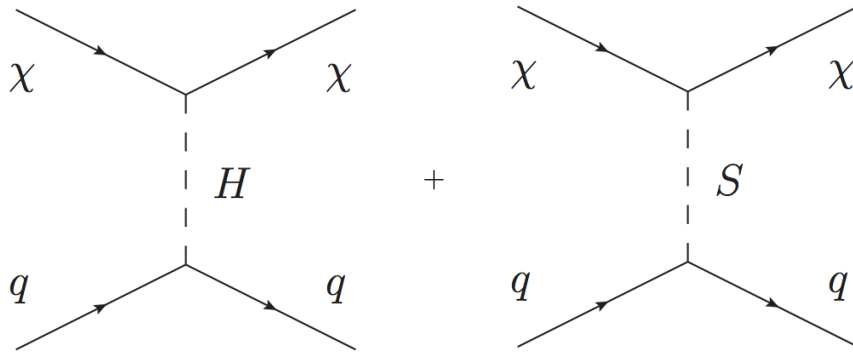


Figure 16: Feynman diagrams for DM-quark scattering.

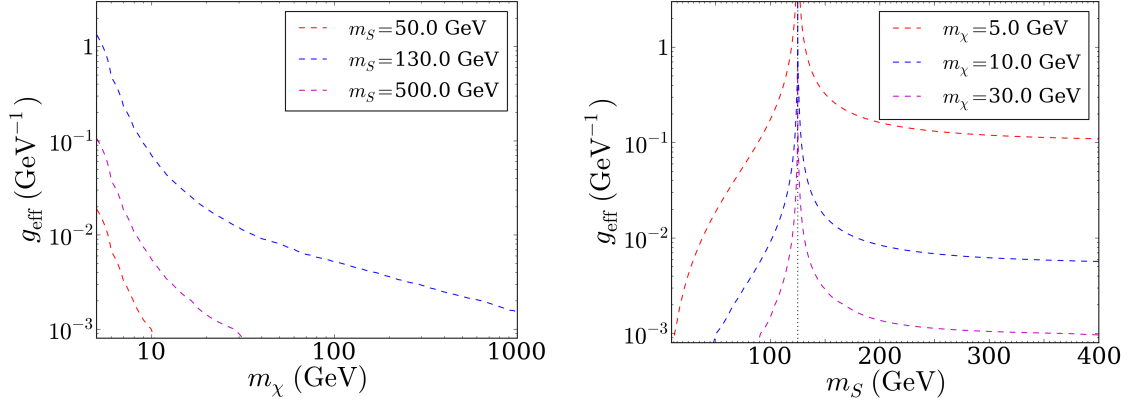


Figure 17: LUX upper limit on the effective coupling $g_{\text{eff}} = s_{\theta_h} c_{\theta_h} / v_2$. The dependence on both the dark matter mass (left) and scalar mass (right) are shown.

6 Direct Detection

In any model that includes a generic weakly interacting massive particle (WIMP), limits inevitably arise from DM direct detection searches. In this case, the spin-independent cross section for DM scattering by nucleons receives a contribution from the Higgs and scalar couplings to the DM candidate χ . The scattering process occurs by t -channel exchange of either H or S . The corresponding Feynman diagrams for the parton subprocesses are shown in figure 16.

The spin-independent cross section for χ -nucleon scattering is then given by

$$\sigma_{SI} = \left(\frac{s_{\theta_h} c_{\theta_h}}{v_2} \right)^2 m_\chi^2 \left(\frac{f_N m_N}{v_1} \right)^2 \frac{\mu^2}{\pi} \left(\frac{1}{m_H^2} - \frac{1}{m_S^2} \right)^2. \quad (6.1)$$

The Higgs coupling to nucleons (rather than partons) is accounted for in the factor $f_N m_N / v_1$, with $f_N = 0.303$ [17]. Here, μ is the χ -nucleon reduced mass, $\mu = m_\chi m_N / (m_\chi + m_N)$ and the difference in proton and neutron mass is assumed negligible, taking $m_N = 0.946$ GeV.

Current results from LUX [112] give the most stringent limit on direct detection of WIMP-nucleon scattering. They present an upper limit at 90% c.l. on the spin-independent cross section, as a function of the WIMP mass. The resulting limit on the effective coupling, denoted $g_{\text{eff}} = s_{\theta_h} c_{\theta_h} / v_2$, and its dependence on both the scalar and DM masses is determined, as shown in figure 17. The upper limit on g_{eff} , based on the LUX 90% c.l. bound, is determined as a function of m_χ , while discretely varying m_S , and vice versa. Discrete values of $m_S = \{50, 130, 500\}$ GeV, and $m_\chi = \{5, 10, 30\}$ GeV are chosen.

Noting first the m_χ dependence of the effective coupling limit, the limit is most stringent for heavier χ , due to the additional factor of m_χ^2 in the scalar-dark matter coupling. The limit relaxes for light χ , roughly less than 10 GeV. Considering the dependence of this limit on the scalar mass, the coupling is more tightly constrained for $m_S \lesssim 100$ GeV, while the limit weakens slightly for heavier $m_S > m_H$. A special case is seen as S approaches the degenerate limit, $m_S \sim m_H$, due to destructive interference of the H and S contributions.

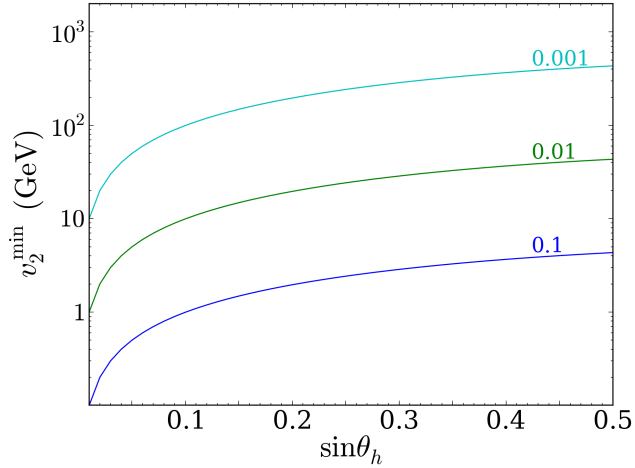


Figure 18: Dependence of the minimum allowed value of v_2 on $\sin \theta_h$, for several values of the upper bound on g_{eff} .

In this narrow region, the upper bound on the coupling is substantially relaxed. For lighter χ , the upper limit on the effective coupling is between $0.01 - 0.1 \text{ GeV}^{-1}$, and can be as large as $\sim 1 \text{ GeV}^{-1}$ for values of m_S near m_H . For heavier χ , this coupling is restricted to be $\mathcal{O}(10^{-3}) \text{ GeV}^{-1}$, or smaller. For illustrative purposes, the dependence of the minimum allowed value of the scalar vev on the value of $\sin \theta_h$ is shown in figure 18, for several maximum values of g_{eff} .

7 Conclusion

Although the current LHC Higgs data are consistent with the Standard Model, there is still the possibility that the observed Higgs could be part of an extended theory, in particular, that a Higgs sector with multiple scalars could be avoiding detection at the current levels of precision. A mixed two-Higgs scenario has been considered, under the addition of a real singlet scalar field to the Standard Model scalar sector. Strict limits from the measured signal strength in LHC Higgs production, and exclusion searches constrain the mixing angle such that the upper bound on $|\sin \theta_h|$ is between 0.3 and 0.5 for various ranges of the scalar mass, above $m_S \sim 80 \text{ GeV}$, while LEP exclusion place a stricter bound for smaller masses, of $|\sin \theta_h| \lesssim 0.15$. For a subset of the parameter space, additional limits arise on the scalar parameters, including the vev of the additional scalar field, from new contributions to the total width of the Higgs, due to decays to a scalar pair. For the case of a light S , the region of scalar parameter space allowed by measurements of the total Higgs width is determined, giving the allowed values of the mixing angle and scalar vev. Smaller values of v_2 , i.e. $v_2 \sim 10 \text{ GeV}$ tend to be disfavoured in this case.

This analysis primarily considered scalar masses of approximately 100 GeV or larger, but masses as low as 1 – 10 GeV were briefly considered in some cases — specifically the contribution to the Higgs width from decays to a scalar pair, and in the region excluded

by LEP data. Although ~ 1 GeV scalar masses were not the focus here, it should be noted that in the region of $m_S \lesssim 4$ GeV, there is potential for the mixing angle to be strictly constrained by recent LHCb data corresponding to a search for hidden-sector bosons in B^0 decays [113].

The model is also extended to include a possible application to dark matter, via the addition of a chiral Yukawa coupling of the scalar singlet to a dark fermion. Two Majorana mass states generally result as the scalar acquires a vev, which are equivalently expressed as a single Dirac fermion in the degenerate case which is considered here. The initial implications of the simpler case of a single dark fermion in this extended Higgs portal framework are investigated, with the extended case of two non-degenerate dark matter species left for future work. Bounds on the Higgs invisible width place limits on the dark sector of the model. Specifically, such measurements constrain the scalar vev to be approximately greater than 100 or 500 GeV, for $\sin \theta_h = 0.1, 0.4$ respectively, for values of m_χ in the region kinematically allowed by the $H \rightarrow \chi\bar{\chi}$ decay. The lower bound on v_2 is relaxed for very light χ , $m_\chi \sim 1$ GeV. Alternatively, the constraint on v_2 is avoided for $m_\chi > m_H/2$. Additional limits on the parameters describing the dark sector interaction are obtained by direct detection results, from H and S mediated contributions to the spin-independent χ -nucleon scattering cross section. The maximally allowed value of the effective coupling, $g_{\text{eff}} = \sin \theta_h \cos \theta_h / v_2$, is determined as a function of the dark matter mass, with additional dependence on the mass of the new scalar. The resulting constraint places a lower bound on the scalar vev, which varies with the values of the mixing angle and masses of S and χ , and disfavors heavier χ . It is noted that possible tension with the LUX result is avoided under three possibilities: either lighter dark matter with $m_\chi \lesssim 10$ GeV, v_2 values of order 1 TeV, or values of m_S which are near the SM Higgs mass.

Under the scenario in which an additional scalar has evaded detection at current hadron colliders, the remaining parameter space is probed in a Higgs precision environment, investigating the discovery potential at ILC. The presence of the additional scalar, and induced mixing, results in unique contributions to the di-Higgs production process. Based on expected precision in measurement of the di-Higgs cross section, it is shown that there exists a measurable region in the remaining allowed parameter space, over which the effect of scalar mixing could be observed. Future experiments in Higgs precision will offer interesting results, and the opportunity to further constrain, or perhaps detect, new physics in the Higgs sector.

A Di-Higgs Production Diagrams

Additional Feynman diagrams contributing to di-Higgs production processes at ILC are given here. Included, are the background diagrams for HHZ production, and the diagrams for $HH\nu_e\bar{\nu}_e$ production, via WW fusion, including both background, and the scalar trilinear and self coupling contributions. It should be noted, that $HH\nu_e\bar{\nu}_e$ production also includes the corresponding Higgs-strahlung diagrams in which the final-state Z decays to $\nu_e\bar{\nu}_e$.

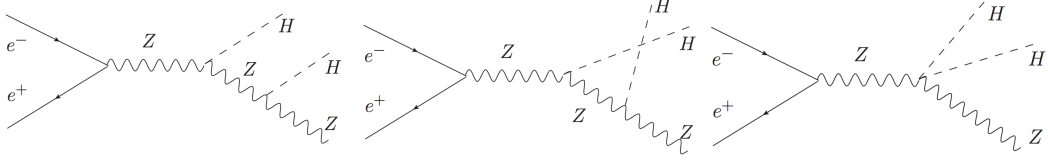


Figure 19: Background diagrams for double Higgs-strahlung process.

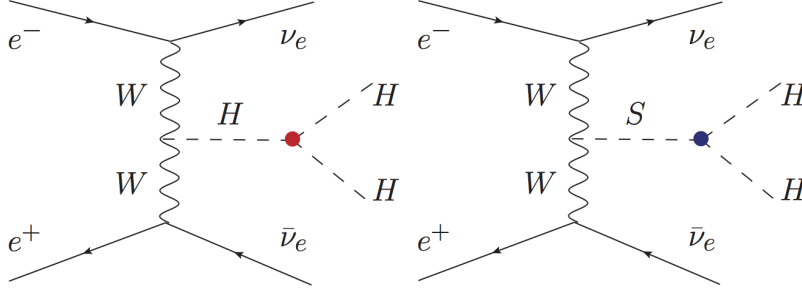


Figure 20: Contribution of Higgs self coupling and mixed scalar coupling to di-Higgs production via WW fusion.

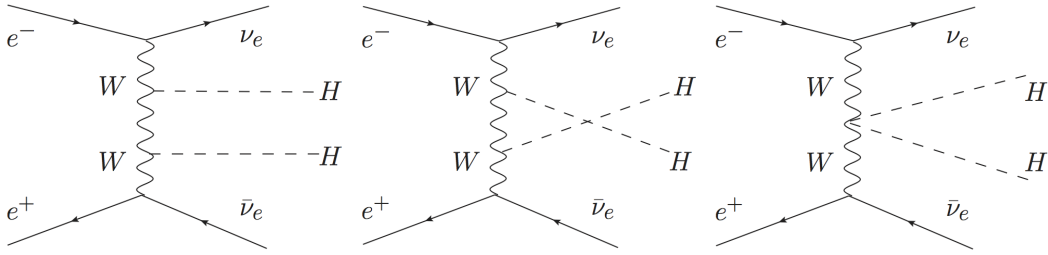


Figure 21: Background diagrams contributing to di-Higgs WW fusion process.

Acknowledgments

The author would like to thank Jim Cline for valuable comments, guidance, and supervision of this project, as well as Brigitte Vachon and Guy Moore for helpful discussions. Research is supported by the Natural Sciences and Engineering Research Council (NSERC) of Canada.

References

- [1] T. Robens and T. Stefaniak, *Status of the Higgs Singlet Extension of the Standard Model after LHC Run 1*, *Eur. Phys. J.* **C75** (2015) 104, [[1501.02234](#)].
- [2] G. M. Pruna and T. Robens, *Higgs singlet extension parameter space in the light of the LHC discovery*, *Phys. Rev.* **D88** (2013) 115012, [[1303.1150](#)].
- [3] S. I. Godunov, A. N. Rozanov, M. I. Vysotsky and E. V. Zhemchugov, *Extending the Higgs sector: an extra singlet*, *Eur. Phys. J.* **C76** (2016) 1, [[1503.01618](#)].

- [4] V. Martı́n Lozano, J. M. Moreno and C. B. Park, *Resonant Higgs boson pair production in the $hh \rightarrow b\bar{b} WW \rightarrow b\bar{b}\ell^+\nu\ell^-\bar{\nu}$ decay channel*, *JHEP* **08** (2015) 004, [[1501.03799](#)].
- [5] A. Falkowski, C. Gross and O. Lebedev, *A second Higgs from the Higgs portal*, *JHEP* **05** (2015) 057, [[1502.01361](#)].
- [6] A. Berlin, S. Gori, T. Lin and L.-T. Wang, *Pseudoscalar Portal Dark Matter*, *Phys. Rev. D* **92** (2015) 015005, [[1502.06000](#)].
- [7] C. Kouvaris, I. M. Shoemaker and K. Tuominen, *Self-Interacting Dark Matter through the Higgs Portal*, *Phys. Rev. D* **91** (2015) 043519, [[1411.3730](#)].
- [8] M. R. Buckley, D. Feld and D. Goncalves, *Scalar Simplified Models for Dark Matter*, *Phys. Rev. D* **91** (2015) 015017, [[1410.6497](#)].
- [9] K. Ghorbani, *Fermionic dark matter with pseudo-scalar Yukawa interaction*, *JCAP* **1501** (2015) 015, [[1408.4929](#)].
- [10] L. Basso, O. Fischer and J. J. van Der Bij, *A renormalization group analysis of the Hill model and its HEIDI extension*, *Phys. Lett. B* **730** (2014) 326–331, [[1309.6086](#)].
- [11] L. Basso, O. Fischer and J. J. van der Bij, *A singlet-triplet extension for the Higgs search at LEP and LHC*, *Europhys. Lett.* **101** (2013) 51004, [[1212.5560](#)].
- [12] M. A. Fedderke, J.-Y. Chen, E. W. Kolb and L.-T. Wang, *The Fermionic Dark Matter Higgs Portal: an effective field theory approach*, *JHEP* **08** (2014) 122, [[1404.2283](#)].
- [13] S. Baek, P. Ko and W.-I. Park, *Search for the Higgs portal to a singlet fermionic dark matter at the LHC*, *JHEP* **02** (2012) 047, [[1112.1847](#)].
- [14] F. S. Queiroz, K. Sinha and A. Strumia, *Leptoquarks, Dark Matter, and Anomalous LHC Events*, *Phys. Rev. D* **91** (2015) 035006, [[1409.6301](#)].
- [15] L. Feng, S. Profumo and L. Ubaldi, *Closing in on singlet scalar dark matter: LUX, invisible Higgs decays and gamma-ray lines*, *JHEP* **03** (2015) 045, [[1412.1105](#)].
- [16] A. Martin, J. Shelton and J. Unwin, *Fitting the Galactic Center Gamma-Ray Excess with Cascade Annihilations*, *Phys. Rev. D* **90** (2014) 103513, [[1405.0272](#)].
- [17] J. M. Cline, K. Kainulainen, P. Scott and C. Weniger, *Update on scalar singlet dark matter*, *Phys. Rev. D* **88** (2013) 055025, [[1306.4710](#)].
- [18] E. Izaguirre, G. Krnjaic and B. Shuve, *The Galactic Center Excess from the Bottom Up*, *Phys. Rev. D* **90** (2014) 055002, [[1404.2018](#)].
- [19] I. Medeiros Varzielas and O. Fischer, *Non-Abelian family symmetries as portals to dark matter*, *JHEP* **01** (2016) 160, [[1512.00869](#)].
- [20] PARTICLE DATA GROUP collaboration, K. A. Olive et al., *Review of Particle Physics*, *Chin. Phys.* **C38** (2014) 090001.
- [21] P. Bechtle, S. Heinemeyer, O. Stal, T. Stefaniak and G. Weiglein, *Applying Exclusion Likelihoods from LHC Searches to Extended Higgs Sectors*, *Eur. Phys. J. C* **75** (2015) 421, [[1507.06706](#)].
- [22] P. Bechtle et al., *HiggsBounds-4: Improved Tests of Extended Higgs Sectors against Exclusion Bounds from LEP, the Tevatron and the LHC*, *Eur. Phys. J. C* **74** (2014) 2693, [[1311.0055](#)].

- [23] P. Bechtle et al., *Recent Developments in HiggsBounds and a Preview of HiggsSignals*, *PoS CHARGED2012* (2012) 024, [[1301.2345](#)].
- [24] P. Bechtle, O. Brein, S. Heinemeyer, G. Weiglein and K. E. Williams, *HiggsBounds 2.0.0: Confronting Neutral and Charged Higgs Sector Predictions with Exclusion Bounds from LEP and the Tevatron*, *Comput. Phys. Commun.* **182** (2011) 2605–2631, [[1102.1898](#)].
- [25] P. Bechtle, O. Brein, S. Heinemeyer, G. Weiglein and K. E. Williams, *HiggsBounds: Confronting Arbitrary Higgs Sectors with Exclusion Bounds from LEP and the Tevatron*, *Comput. Phys. Commun.* **181** (2010) 138–167, [[0811.4169](#)].
- [26] LEP HIGGS WORKING GROUP FOR HIGGS BOSON SEARCHES collaboration, *Flavor independent search for hadronically decaying neutral Higgs bosons at LEP*, in *Lepton and photon interactions at high energies. Proceedings, 20th International Symposium, LP 2001, Rome, Italy, July 23-28, 2001*, 2001. [hep-ex/0107034](#).
- [27] OPAL collaboration, G. Abbiendi et al., *Decay mode independent searches for new scalar bosons with the OPAL detector at LEP*, *Eur. Phys. J.* **C27** (2003) 311–329, [[hep-ex/0206022](#)].
- [28] OPAL, DELPHI, LEP HIGGS WORKING FOR HIGGS BOSON SEARCHES, L3 CERN, ALEPH collaboration, *Searches for invisible Higgs bosons: Preliminary combined results using LEP data collected at energies up to 209-GeV*, in *Lepton and photon interactions at high energies. Proceedings, 20th International Symposium, LP 2001, Rome, Italy, July 23-28, 2001*, 2001. [hep-ex/0107032](#).
- [29] DELPHI collaboration, J. Abdallah et al., *Searches for invisibly decaying Higgs bosons with the DELPHI detector at LEP*, *Eur. Phys. J.* **C32** (2004) 475–492, [[hep-ex/0401022](#)].
- [30] OPAL collaboration, G. Abbiendi et al., *Search for invisibly decaying Higgs bosons in $e^+e^- \rightarrow Z_0 h_0$ production at $\sqrt{s} = 183 - 209$ GeV*, *Phys. Lett.* **B682** (2010) 381–390, [[0707.0373](#)].
- [31] OPAL, DELPHI, L3, ALEPH, LEP HIGGS WORKING GROUP FOR HIGGS BOSON SEARCHES collaboration, *Search for charged Higgs bosons: Preliminary combined results using LEP data collected at energies up to 209-GeV*, in *Lepton and photon interactions at high energies. Proceedings, 20th International Symposium, LP 2001, Rome, Italy, July 23-28, 2001*, 2001. [hep-ex/0107031](#).
- [32] OPAL collaboration, G. Abbiendi et al., *Search for Yukawa production of a light neutral Higgs boson at LEP*, *Eur. Phys. J.* **C23** (2002) 397–407, [[hep-ex/0111010](#)].
- [33] L3 collaboration, P. Achard et al., *Search for an invisibly-decaying Higgs boson at LEP*, *Phys. Lett.* **B609** (2005) 35–48, [[hep-ex/0501033](#)].
- [34] DELPHI, OPAL, ALEPH, LEP WORKING GROUP FOR HIGGS BOSON SEARCHES, L3 collaboration, S. Schael et al., *Search for neutral MSSM Higgs bosons at LEP*, *Eur. Phys. J.* **C47** (2006) 547–587, [[hep-ex/0602042](#)].
- [35] DELPHI collaboration, J. Abdallah et al., *Search for charged Higgs bosons at LEP in general two Higgs doublet models*, *Eur. Phys. J.* **C34** (2004) 399–418, [[hep-ex/0404012](#)].
- [36] DELPHI collaboration, J. Abdallah et al., *Searches for neutral higgs bosons in extended models*, *Eur. Phys. J.* **C38** (2004) 1–28, [[hep-ex/0410017](#)].
- [37] ATLAS collaboration, “ATLAS CONF notes 2012-160 2014-049 2012-135 2012-161

2012-092 2012-018 2012-012 2013-010 2013-013 2012-019 2012-168 2012-078 2014-050
2012-017 2012-016 2011-094 2013-030 2011-157.”

- [38] LEP Higgs Working Group, “LHWG notes 2002-02.”
- [39] ATLAS collaboration, G. Aad et al., *Search for the Standard Model Higgs boson decay to $\mu^+\mu^-$ with the ATLAS detector*, *Phys. Lett. B* **738** (2014) 68–86, [[1406.7663](#)].
- [40] CMS collaboration, S. Chatrchyan et al., *Search for a Higgs boson in the decay channel $H \rightarrow ZZ^* \rightarrow q\bar{q}\ell^-\ell^+$ in pp collisions at $\sqrt{s} = 7$ TeV*, *JHEP* **04** (2012) 036, [[1202.1416](#)].
- [41] CMS collaboration, S. Chatrchyan et al., *Search for invisible decays of Higgs bosons in the vector boson fusion and associated ZH production modes*, *Eur. Phys. J. C* **74** (2014) 2980, [[1404.1344](#)].
- [42] ATLAS collaboration, G. Aad et al., *Observation of a new particle in the search for the Standard Model Higgs boson with the ATLAS detector at the LHC*, *Phys. Lett. B* **716** (2013) 1–29, [[1207.7214](#)].
- [43] ATLAS collaboration, G. Aad et al., *Search for charged Higgs bosons decaying via $H^\pm \rightarrow \tau\nu$ in top quark pair events using pp collision data at $\sqrt{s} = 7$ TeV with the ATLAS detector*, *JHEP* **06** (2012) 039, [[1204.2760](#)].
- [44] CMS collaboration, S. Chatrchyan et al., *Combined results of searches for the standard model Higgs boson in pp collisions at $\sqrt{s} = 7$ TeV*, *Phys. Lett. B* **710** (2013) 26–48, [[1202.1488](#)].
- [45] ATLAS collaboration, G. Aad et al., *Search for a heavy Standard Model Higgs boson in the channel $H \rightarrow ZZ \rightarrow \ell\ell q\bar{q}$ using the ATLAS detector*, *Phys. Lett. B* **707** (2013) 27–45, [[1108.5064](#)].
- [46] ATLAS collaboration, G. Aad et al., *Search for the Standard Model Higgs boson in the decay channel $H \rightarrow ZZ(*) \rightarrow 4\ell$ with 4.8 fb^{-1} of pp collision data at $\sqrt{s} = 7$ TeV with ATLAS*, *Phys. Lett. B* **710** (2013) 383–402, [[1202.1415](#)].
- [47] ATLAS collaboration, G. Aad et al., *Search for a Standard Model Higgs boson in the $H \rightarrow ZZ \rightarrow \ell^+\ell^-\nu\bar{\nu}$ decay channel with the ATLAS detector*, *Phys. Rev. Lett.* **107** (2011) 221802, [[1109.3357](#)].
- [48] CMS collaboration, V. Khachatryan et al., *Search for neutral MSSM Higgs bosons decaying to a pair of tau leptons in pp collisions*, *JHEP* **10** (2014) 160, [[1408.3316](#)].
- [49] ATLAS collaboration, G. Aad et al., *Search for the Higgs boson in the $H \rightarrow WW \rightarrow \ell\nu jj$ decay channel in pp collisions at $\sqrt{s} = 7$ TeV with the ATLAS detector*, *Phys. Rev. Lett.* **107** (2011) 231801, [[1109.3615](#)].
- [50] CMS collaboration, S. Chatrchyan et al., *Search for the standard model Higgs boson in the decay channel $H \rightarrow ZZ \rightarrow 4\ell$ in pp collisions at $\sqrt{s} = 7$ TeV*, *Phys. Rev. Lett.* **108** (2012) 111804, [[1202.1997](#)].
- [51] ATLAS collaboration, G. Aad et al., *Search for Higgs boson decays to a photon and a Z boson in pp collisions at $\sqrt{s}=7$ and 8 TeV with the ATLAS detector*, *Phys. Lett. B* **732** (2014) 8–27, [[1402.3051](#)].
- [52] ATLAS collaboration, G. Aad et al., *Search For Higgs Boson Pair Production in the $\gamma\gamma b\bar{b}$ Final State using pp Collision Data at $\sqrt{s} = 8$ TeV from the ATLAS Detector*, *Phys. Rev. Lett.* **114** (2015) 081802, [[1406.5053](#)].

- [53] ATLAS collaboration, G. Aad et al., *Search for Invisible Decays of a Higgs Boson Produced in Association with a Z Boson in ATLAS*, *Phys. Rev. Lett.* **112** (2014) 201802, [[1402.3244](#)].
- [54] ATLAS collaboration, G. Aad et al., *Search for neutral MSSM Higgs bosons decaying to $\tau^+\tau^-$ pairs in proton-proton collisions at $\sqrt{s} = 7$ TeV with the ATLAS detector*, *Phys. Lett. B* **705** (2013) 174–192, [[1107.5003](#)].
- [55] ATLAS collaboration, G. Aad et al., *Search for the Higgs boson in the $H \rightarrow WW(*) \rightarrow \ell_\nu \ell_\nu$ decay channel in pp collisions at $\sqrt{s} = 7$ TeV with the ATLAS detector*, *Phys. Rev. Lett.* **108** (2012) 111802, [[1112.2577](#)].
- [56] ATLAS collaboration, G. Aad et al., *Search for the Standard Model Higgs boson in the diphoton decay channel with 4.9 fb^{-1} of pp collisions at $\sqrt{s} = 7$ TeV with ATLAS*, *Phys. Rev. Lett.* **108** (2012) 111803, [[1202.1414](#)].
- [57] CMS collaboration, S. Chatrchyan et al., *Search for a Higgs boson decaying into a Z and a photon in pp collisions at $\sqrt{s} = 7$ and 8 TeV*, *Phys. Lett. B* **726** (2013) 587–609, [[1307.5515](#)].
- [58] ATLAS collaboration, G. Aad et al., *Combined search for the Standard Model Higgs boson using up to 4.9 fb^{-1} of pp collision data at $\sqrt{s} = 7$ TeV with the ATLAS detector at the LHC*, *Phys. Lett. B* **710** (2013) 49–66, [[1202.1408](#)].
- [59] ATLAS collaboration, G. Aad et al., *Search for Scalar Diphoton Resonances in the Mass Range 65 – 600 GeV with the ATLAS Detector in pp Collision Data at $\sqrt{s} = 8$ TeV*, *Phys. Rev. Lett.* **113** (2014) 171801, [[1407.6583](#)].
- [60] CMS collaboration, S. Chatrchyan et al., *Search for the standard model Higgs boson in the H to ZZ to $2\ell 2\nu$ channel in pp collisions at $\sqrt{s} = 7$ TeV*, *JHEP* **03** (2012) 040, [[1202.3478](#)].
- [61] CDF collaboration, “CDF notes 10500 7307 10439 10796 9999 10485 10798 8353 10799 10599 10573 10010 7712 10574.”
- [62] D0 collaboration, “D0 notes 6083 6305 6227 6299 6301 6302 5739 5845 6286 5757 6296 6183 6295 6171 6309 6276 6304 5873.”
- [63] D0 collaboration, V. M. Abazov et al., *Search for neutral Higgs bosons in the multi-b-jet topology in 5.2 fb^{-1} of $p\bar{p}$ collisions at $\sqrt{s} = 1.96$ TeV*, *Phys. Lett. B* **698** (2014) 97–104, [[1011.1931](#)].
- [64] CDF collaboration, T. Aaltonen et al., *Search for Higgs bosons predicted in two-Higgs-doublet models via decays to tau lepton pairs in 1.96-TeV p anti-p collisions*, *Phys. Rev. Lett.* **103** (2009) 201801, [[0906.1014](#)].
- [65] D0 collaboration, V. M. Abazov et al., *Search for $ZH \rightarrow \ell^+ \ell^- b\bar{b}$ production in 4.2 fb^{-1} of $p\bar{p}$ collisions at $\sqrt{s} = 1.96$ TeV*, *Phys. Rev. Lett.* **105** (2010) 251801, [[1008.3564](#)].
- [66] CDF collaboration, T. Aaltonen et al., *Search for Higgs Bosons Produced in Association with b-quarks*, *Phys. Rev. D* **85** (2012) 032005, [[1106.4782](#)].
- [67] CDF collaboration, T. Aaltonen et al., *Inclusive Search for Standard Model Higgs Boson Production in the WW Decay Channel using the CDF II Detector*, *Phys. Rev. Lett.* **104** (2010) 061803, [[1001.4468](#)].
- [68] TEVNPH WORKING GROUP (TEVATRON NEW PHENOMENA AND HIGGS WORKING GROUP), CDF, D0 collaboration, D. Benjamin, *Combined CDF and D0 upper limits on $gg \rightarrow H \rightarrow W^+W^-$ and constraints on the Higgs boson mass in fourth-generation fermion*

- models with up to 8.2 fb^{-1} of data, in *Proceedings, 21st International Europhysics Conference on High energy physics (EPS-HEP 2011)*, 2011. [1108.3331](#).
- [69] TEVATRON NEW PHYSICS HIGGS WORKING GROUP, CDF, D0 collaboration, *Updated Combination of CDF and D0 Searches for Standard Model Higgs Boson Production with up to 10.0 fb^{-1} of Data*, 2012. [1207.0449](#).
 - [70] CDF collaboration, T. Aaltonen et al., *Search for charged Higgs bosons in decays of top quarks in $p - \bar{p}$ collisions at $\sqrt{s} = 1.96 \text{ TeV}$* , *Phys. Rev. Lett.* **103** (2009) 101803, [[0907.1269](#)].
 - [71] D0 collaboration, V. M. Abazov et al., *Search for neutral Minimal Supersymmetric Standard Model Higgs bosons decaying to tau pairs produced in association with b quarks in $p\bar{p}$ collisions at $\sqrt{s} = 1.96 \text{ TeV}$* , *Phys. Rev. Lett.* **107** (2011) 121801, [[1106.4885](#)].
 - [72] D0 collaboration, V. M. Abazov et al., *Search for a scalar or vector particle decaying into $Z\gamma$ in $p\bar{p}$ collisions at $\sqrt{s}=1.96 \text{ TeV}$* , *Phys. Lett.* **B671** (2009) 349–355, [[0806.0611](#)].
 - [73] CDF, D0 collaboration, T. Aaltonen et al., *Evidence for a particle produced in association with weak bosons and decaying to a bottom-antibottom quark pair in Higgs boson searches at the Tevatron*, *Phys. Rev. Lett.* **109** (2012) 071804, [[1207.6436](#)].
 - [74] D0 collaboration, V. M. Abazov et al., *Search for NMSSM Higgs bosons in the $h \rightarrow aa \rightarrow \mu\mu\mu\mu, \mu\mu\tau\tau$ channels using $p\bar{p}$ collisions at $\sqrt{s} = 1.96 \text{ TeV}$* , *Phys. Rev. Lett.* **103** (2009) 061801, [[0905.3381](#)].
 - [75] TEVATRON NEW PHENOMENA AND HIGGS WORKING GROUP collaboration, D. Benjamin et al., *Combined CDF and D0 Upper Limits on MSSM Higgs Boson Production in tau-tau Final States with up to 2.2 fb^{-1}* , [1003.3363](#).
 - [76] D0 collaboration, V. M. Abazov et al., *Search for Higgs bosons decaying to $\tau\tau$ pairs in $p\bar{p}$ collisions at $\sqrt{s} = 1.96 \text{ TeV}$* , *Phys. Lett.* **B707** (2012) 323–329, [[1106.4555](#)].
 - [77] D0 collaboration, V. M. Abazov et al., *Search for associated Higgs boson production using like charge dilepton events in $p\bar{p}$ collisions at $\sqrt{s} = 1.96 \text{ TeV}$* , *Phys. Rev.* **D84** (2011) 092002, [[1107.1268](#)].
 - [78] CDF, D0 collaboration, T. W. Group, *Combined CDF and D0 Searches for the Standard Model Higgs Boson Decaying to Two Photons with up to 8.2 fb^{-1}* , in *Proceedings, 21st International Europhysics Conference on High energy physics (EPS-HEP 2011)*, 2011. [1107.4960](#).
 - [79] D0 collaboration, V. M. Abazov et al., *Search for WH associated production in 5.3 fb^{-1} of $p\bar{p}$ collisions at the Fermilab Tevatron*, *Phys. Lett.* **B698** (2011) 6–13, [[1012.0874](#)].
 - [80] CDF collaboration, T. Aaltonen et al., *Search for a Higgs Boson Decaying to Two W Bosons at CDF*, *Phys. Rev. Lett.* **102** (2009) 021802, [[0809.3930](#)].
 - [81] CDF collaboration, T. Aaltonen et al., *Search for a Higgs Boson in $WH \rightarrow \ell\nu b\bar{b}$ in $p\bar{p}$ Collisions at $\sqrt{s} = 1.96 \text{ TeV}$* , *Phys. Rev. Lett.* **103** (2009) 101802, [[0906.5613](#)].
 - [82] D0 collaboration, V. M. Abazov et al., *Search for charged Higgs bosons in top quark decays*, *Phys. Lett.* **B682** (2009) 278–286, [[0908.1811](#)].
 - [83] D0 collaboration, V. M. Abazov et al., *Search for Higgs boson production in dilepton and missing energy final states with 5.4 fb^{-1} of $p\bar{p}$ collisions at $\sqrt{s} = 1.96 \text{ TeV}$* , *Phys. Rev. Lett.* **104** (2010) 061804, [[1001.4481](#)].

- [84] D0 collaboration, V. M. Abazov et al., *Search for Resonant Diphoton Production with the D0 Detector*, *Phys. Rev. Lett.* **102** (2009) 231801, [[0901.1887](#)].
- [85] ATLAS collaboration, G. Aad et al., *Search for neutral Higgs bosons of the minimal supersymmetric standard model in pp collisions at $\sqrt{s} = 8$ TeV with the ATLAS detector*, *JHEP* **11** (2014) 056, [[1409.6064](#)].
- [86] ATLAS collaboration, *Searches for Higgs boson pair production in the $hh \rightarrow b\bar{b}\tau\tau, \gamma\gamma WW^*, \gamma\gamma b\bar{b}, b\bar{b}b\bar{b}$ channels with the ATLAS detector*, [1509.04670](#).
- [87] CMS collaboration, *Search for diphoton resonances in the mass range from 150 to 850 GeV in pp collisions at $\sqrt{s} = 8$ TeV*, *Phys. Lett.* **B750** (2015) 494, [[1506.02301](#)].
- [88] CMS collaboration, *Search for a Higgs boson in the mass range from 145 to 1000 GeV decaying to a pair of W or Z bosons*, [1504.00936](#).
- [89] ATLAS collaboration, *Search for an additional, heavy Higgs boson in the $H \rightarrow ZZ$ decay channel at $\sqrt{s} = 8$ TeV in pp collision data with the ATLAS detector*, [1507.05930](#).
- [90] ATLAS collaboration, *Search for a high-mass Higgs boson decaying to a W boson pair in pp collisions at $\sqrt{s} = 8$ TeV with the ATLAS detector*, [1509.00389](#).
- [91] O. Stål and T. Stefaniak, *Constraining extended Higgs sectors with HiggsSignals*, *PoS EPS-HEP2013* (2013) 314, [[1310.4039](#)].
- [92] P. Bechtle, S. Heinemeyer, O. Stål, T. Stefaniak and G. Weiglein, *HiggsSignals: Confronting arbitrary Higgs sectors with measurements at the Tevatron and the LHC*, *Eur. Phys. J.* **C74** (2014) 2711, [[1305.1933](#)].
- [93] ATLAS collaboration, G. Aad et al., *Measurements of the Higgs boson production and decay rates and coupling strengths using pp collision data at $\sqrt{s} = 7$ and 8 TeV in the ATLAS experiment*, [1507.04548](#).
- [94] ATLAS collaboration, G. Aad et al., *Measurement of Higgs boson production in the diphoton decay channel in pp collisions at center-of-mass energies of 7 and 8 TeV with the ATLAS detector*, *Phys. Rev.* **D90** (2014) 112015, [[1408.7084](#)].
- [95] ATLAS collaboration, G. Aad et al., *Evidence for the Higgs-boson Yukawa coupling to tau leptons with the ATLAS detector*, *JHEP* **04** (2015) 117, [[1501.04943](#)].
- [96] ATLAS collaboration, G. Aad et al., *Observation and measurement of Higgs boson decays to WW^* with the ATLAS detector*, *Phys. Rev.* **D92** (2015) 012006, [[1412.2641](#)].
- [97] ATLAS collaboration, ATLAS, *Study of the Higgs boson decaying to WW^* produced in association with a weak boson with the ATLAS detector at the LHC*, 2015.
- [98] ATLAS collaboration, G. Aad et al., *Measurements of Higgs boson production and couplings in the four-lepton channel in pp collisions at center-of-mass energies of 7 and 8 TeV with the ATLAS detector*, *Phys. Rev.* **D91** (2015) 012006, [[1408.5191](#)].
- [99] ATLAS collaboration, G. Aad et al., *Search for the $b\bar{b}$ decay of the Standard Model Higgs boson in associated $(W/Z)H$ production with the ATLAS detector*, *JHEP* **01** (2015) 069, [[1409.6212](#)].
- [100] CMS collaboration, V. Khachatryan et al., *Observation of the diphoton decay of the Higgs boson and measurement of its properties*, *Eur. Phys. J.* **C74** (2014) 3076, [[1407.0558](#)].
- [101] CMS collaboration, S. Chatrchyan et al., *Evidence for the direct decay of the 125 GeV Higgs boson to fermions*, *Nature Phys.* **10** (2014) 557–560, [[1401.6527](#)].

- [102] CMS collaboration, S. Chatrchyan et al., *Measurement of Higgs boson production and properties in the WW decay channel with leptonic final states*, *JHEP* **01** (2014) 096, [[1312.1129](#)].
- [103] CMS collaboration, S. Chatrchyan et al., *Measurement of the properties of a Higgs boson in the four-lepton final state*, *Phys. Rev.* **D89** (2014) 092007, [[1312.5353](#)].
- [104] CMS COLLABORATION collaboration, CMS, *Combination of standard model Higgs boson searches and measurements of the properties of the new boson with a mass near 125 GeV*, 2013.
- [105] ATLAS collaboration, G. Aad et al., *Constraints on new phenomena via Higgs boson couplings and invisible decays with the ATLAS detector*, [1509.00672](#).
- [106] CMS collaboration, V. Khachatryan et al., *Limits on the Higgs boson lifetime and width from its decay to four charged leptons*, [1507.06656](#).
- [107] J. Alwall, R. Frederix, S. Frixione, V. Hirschi, F. Maltoni, O. Mattelaer et al., *The automated computation of tree-level and next-to-leading order differential cross sections, and their matching to parton shower simulations*, *JHEP* **07** (2014) 079, [[1405.0301](#)].
- [108] T. Behnke et al., *The International Linear Collider Technical Design Report - Volume 1: Executive Summary*, [1306.6327](#).
- [109] A. Alloul, N. D. Christensen, C. Degrande, C. Duhr and B. Fuks, *FeynRules 2.0 - A complete toolbox for tree-level phenomenology*, *Comput. Phys. Commun.* **185** (2014) 2250–2300, [[1310.1921](#)].
- [110] H. Baer et al., *The International Linear Collider Technical Design Report - Volume 2: Physics*, [1306.6352](#).
- [111] J. Tian, *Study of the Higgs self-coupling at the ILC based on full detector simulation at $\sqrt{s} = 500$ GeV and $\sqrt{s} = 1$ TeV*, 2013.
- [112] LUX collaboration, D. S. Akerib et al., *Improved WIMP scattering limits from the LUX experiment*, [1512.03506](#).
- [113] LHCb collaboration, R. Aaij et al., *Search for hidden-sector bosons in $B^0 \rightarrow K^{*0} \mu^+ \mu^-$ decays*, *Phys. Rev. Lett.* **115** (2015) 161802, [[1508.04094](#)].